
Amenable Sparse Network Investigator

Saeed Damadi, Erfan nouri, and Hamed Pirsavash

Department of Computer Science and Electrical Engineering
University of Maryland, Baltimore County
Baltimore, MD 21250

sdamadi1@umbc.edu, erfan1@umbc.edu, hpirsiav@umbc.edu

Abstract

As the optimization problem of pruning a neural network is nonconvex and the strategies are only guaranteed to find local solutions, a good initialization becomes paramount. To this end, we present the Amenable Sparse Network Investigator (*ASNI*) algorithm that learns a sparse network whose initialization is compressed. The learned sparse structure found by *ASNI* is *amenable* since its corresponding initialization, which is also learned by *ASNI*, consists of only $2L$ numbers, where L is the number of layers. Requiring just a few numbers for parameter initialization of the learned sparse network makes the sparse network *amenable*. The learned initialization set consists of L signed pairs that act as the centroids of parameter values of each layer. These centroids are learned by the *ASNI* algorithm after only one single round of training. We experimentally show that the learned centroids are sufficient to initialize the nonzero parameters of the learned sparse structure in order to achieve approximately the accuracy of non-sparse network. We also empirically show that in order to learn the centroids, one needs to prune the network globally and gradually. Hence, for parameter pruning we propose a novel strategy based on a sigmoid function that specifies the sparsity percentage across the network globally. Then, pruning is done magnitude-wise and after each epoch of training. We have performed a series of experiments utilizing networks such as ResNets, VGG-style, small convolutional, and fully connected ones on ImageNet, CIFAR10, and MNIST datasets.

1 Introduction

Pruning of a neural network is done for two main purposes: (1) obtaining an accurate sparse network, ready to use, whose test accuracy is on a par with the dense version of the network, and (2) finding trainable sparse structures that can be trained in isolation and can reach test accuracy of the dense network. The first purpose has almost been fulfilled, but the second one is still a work in progress.

Working on the first objective started more than 30 years ago (Hanson and Pratt, 1989; LeCun et al., 1990; Hassibi and Stork, 1993). However for deep neural networks, initially Han et al. (2015b) showed that it is possible to achieve off the shelf sparse networks simply by magnitude-wise pruning. Since then, many works have been done using this concept (Han et al., 2015a; Wen et al., 2016; Guo et al., 2016; Molchanov et al., 2016; Li et al., 2016; Zhu and Gupta, 2017; Narang et al., 2017; Luo et al., 2017; Louizos et al., 2017; Liu et al., 2018; Tartaglione et al., 2018; Mocanu et al., 2018; Dettmers and Zettlemoyer, 2019; Mostafa and Wang, 2019; Kusupati et al., 2020).

The second purpose of pruning is to find a sparse network that can fit the training data from scratch. A practical way of finding a sparse trainable network is to first find a mask and then show that the associated sparse network is trainable from a specific sparse initialization that is determined by the learned mask. This is how the *lottery ticket algorithm* works (Frankle and Carbin, 2018). Thanks to this algorithm, search for finding a sparse trainable network has attracted a lot of attention recently.

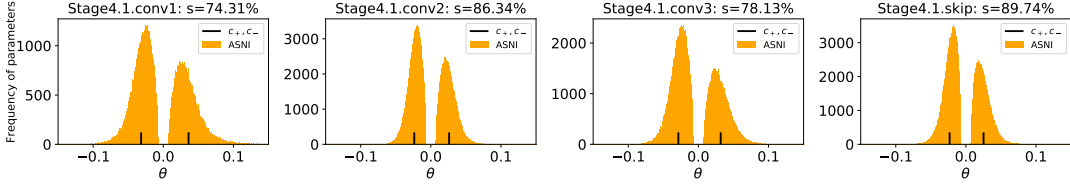


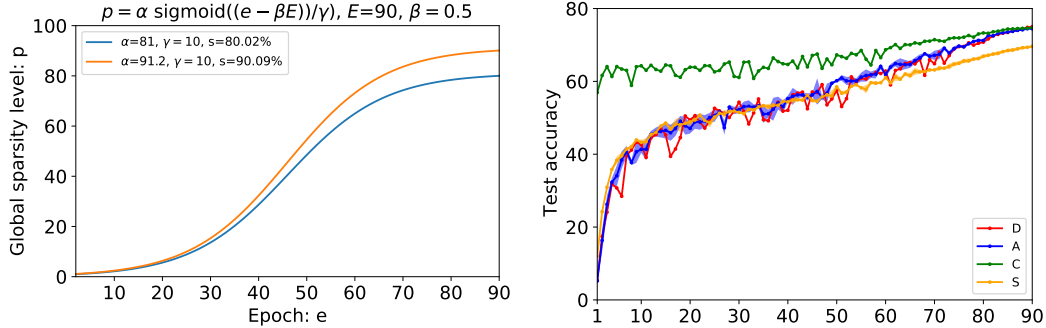
Figure 1: Parameter distribution of ResNet-50 trained on ImageNet with *ASNI*. ResNet-50 has 4 main stages where stages have 3, 4, 6, and 3 bottlenecks, respectively. The first bottleneck of each stage has 3 convolution layers and a skip connection. This picture shows parameter distribution of the first bottleneck in the forth stage at overall sparsity percentage of $s = 80\%$. Two short bars indicate c_+ and c_- for each layer that are used for the initialization of the learned amenable sparse network. To see all stages of the network, check Appendix B.

Unfortunately, there are three issues with the *lottery ticket algorithm*. First, it requires multiple rounds of training. Second, it fails to find the ticket for large networks. Third, it does not provide a strategy to increase sparsity at each round rather than keeping the sparsity percentage as a constant. Foresight pruning or pruning before training (Lee et al., 2018; Wang et al., 2020; Tanaka et al., 2020) tries to address the first issue. However, it does not perform as good as sparse structures found from gradual pruning (Gale et al., 2019; Frankle et al., 2019). In order to alleviate the second problem the authors changed its definition from what was postulated in (Frankle and Carbin, 2018) to another one that is defined in (Frankle et al., 2019). This change is just using another sparse initialization which uses parameters from the k -th step of the optimization. We will elaborate on this fact in Subsection (3.2). To resolve the third issue, Savarese et al. (2019) present an algorithmic way that continuously discards unimportant non-zero parameters. This is achieved at the expense of doubling the number of parameters and by incorporating new learnable parameters for every parameter of the network.

Our goal is to resolve all the three issues with the *lottery ticket algorithm* at once. To this end, we present the “Amenable Sparse Network Investigator” (*ASNI*) algorithm that utilizes a novel pruning strategy based on a sigmoid function. *ASNI* learns the sparse structure in only one round of training. It also learns the corresponding sparse initialization from which the network can be trained to reach test accuracy of the dense network approximately. The initialization that we propose is a compressed set of $2L$ numbers where L is the number of layers. To the best of our knowledge, our proposed initialization set is the first sparse and compressed initialization which only needs $2L$ numbers. In summary, the following are our contributions:

- We present the “Amenable Sparse Network Investigator” (*ASNI*) algorithm that utilizes a novel pruning strategy based on a sigmoid function that induces sparsity level globally over the course of one single round of training. Figure (2a) shows the global sparsity level at each epoch for finding a sparse network out of ResNet-50 structure trained on the ImageNet-1K.
- In only one single training round, *ASNI* learns a trainable sparse architecture by learning a binary mask vector where zero entries are associated with parameters that should be pruned.
- At the end of one training round, *ASNI* learns pairs of signed centroids for each layer (positive and negative), i.e., $\bar{c}_+^{[l]}, \bar{c}_-^{[l]}$. Once they are replaced instead of every positive and negative learned parameters of each layer respectively, the new parameter vector becomes a learned sparse initialization. We experimentally show that these learned centroids are in fact concentration points of parameters in each layer of the trained network which has been sparsified gradually by the *ASNI* during training. In other words, for each layer there are two distinct normal-like distributions whose means are the learned centroids. Figure (1) shows parameter distribution and centroids for ResNet-50. This pattern repeats for all experiments.
- Finally, as shown in Figure (2b) and Table 2, we experimentally show that the learned sparse structure equipped with the learned compressed sparse initialization approximately achieves the test accuracy of the the dense network.

Our work shares the same spirit as Frankle et al. (2019) and Savarese et al. (2019), but differs from them since *ASNI* avoids multiple rounds of training to find the mask. Also, as opposed to Savarese et al. (2019) which doubles the number of parameters, *ASNI* maintains the parameter count. Furthermore, in contrast to pruning at initialization (Lee et al., 2018; Wang et al., 2020; Tanaka et al., 2020), *ASNI* reaches virtually the same accuracy as the dense network. Finally, the distinction between our method and Kusupati et al. (2020) and Evci et al. (2020) is that *ASNI* uses the global



(a) Sigmoid functions
Figure 2: Figure (2a) shows sparsity percentages at each epoch of training of a ResNet50 network on ImageNet-1K for $s \approx 80, 90\%$. This percentage is the global sparsity percentage, not the sparsity of each layer. Look at Figure (4) to see how sparsity is distributed over all layers. Due to this sparsity strategy, the network is allowed to learn the main structure at the early stages of pruning. This strategy lets the network learn with full capacity until almost 5-th epoch. Until then the network sparsity has to be very small. After that, pruning increases with a small slope until almost 35-th epoch. Once *ASNI* makes sure that the network has learned the main structure, the slope increases until 60-th epoch. From that point on, the sparsity level decreases to recover from all the previous pruning and reaches the maximum allowed sparsity percentage slowly. Figure (2b) compares test accuracy of four ResNet50 networks at each epoch: (D) dense network with $s = 0$, (A) trained with *ASNI* to have $s \approx 80\%$, (C) sparse network ($s \approx 80\%$) reinitialized by *ASNI* initialization (c_{\pm}), and (S) sparse network ($s \approx 80\%$) reinitialized by the original initialization. *ASNI* can sparsify the network in a way that final test accuracy of the learned sparse network is approximately equal to that of the dense network. The learned sparse network initialized by the *ASNI* approximately reaches test accuracy of the dense network but the one initialized by the original initialization cannot.

pruning approach to find a trainable sparse network, while both of these methods apply layer-wise pruning.

2 Related Work

Although neural networks are over-parameterized (Denil et al., 2013), they have been able to solve many difficult problems. Due to the huge number of parameters, interpretability of parameters in different layers is not straight-forward. This is why neural networks are considered black boxes most of the time. Simpler models are easier to explain. Therefore, finding a sparse network that can fit to a data from scratch would help to interpret parameters of a neural network. To this end, Frankle and Carbin (2018) showed that typical dense neural networks contain a small sparse sub-network that can be trained to reach similar test accuracy in an equal number of steps. However, their method was not able to find tickets for large networks. Hence, Frankle et al. (2019) use parameters of the k -th step as the initialization to reach test accuracy of the dense network. Rewinding to an intermediate step k in order to obtain a sparse trainable network has also been observed by You et al. (2019). Necessity for rewinding to the k -th step utilized by Frankle et al. (2019) and You et al. (2019) corroborates the observation in Achille et al. (2018) that in the early stages of training, important connectivity patterns between layers are first discovered, which stay relatively fixed in the later steps of training.

The *lottery ticket algorithm* has an uncomplicated strategy to force more sparsity to the network by just applying a specific percentage at each round of training. This strategy can be improved as Savarese et al. (2019) use a continuous strategy to remove parameters at each round of training. However, this is done at the expense of doubling the number of parameters which is not efficient.

Frankle and Carbin (2018), Frankle et al. (2019), and Savarese et al. (2019) all search for the sparse structure utilizing multiple rounds of training which is very costly. The best way could be by finding a sparse structure even before training. This is called foresight pruning or pruning before training. To this end, Lee et al. (2018) (SNIP) was the first work that posited the idea of foresight pruning which is performed as a single shot of pruning. In this approach, a *connection sensitivity* score is calculated before training and parameters are removed based on the score vector. Others have tried to find different scoring vectors. For example, Wang et al. (2020) introduce GraSP, utilizing Hessian-gradient product to find a score vector. See Appendix A.1 for more information about scoring vectors. As

opposed to the previous proposed methods, Tanaka et al. (2020) find a sparse structure using different scoring in n rounds of pruning. All of the above aforementioned methods make use of the dense initialization to calculate the gradient or Hessian-gradient in order to find the score vector. Therefore, the mask would be a random vector and can be different from one initialization to another.

It is true that finding the sparse structure before training is the ideal approach and may have a negligible computational cost to find a mask, but the performance of the methods that apply pruning before training is not competitive with performance of networks whose initialization is obtained using pruning far later in training (Gale et al., 2019; Frankle et al., 2020). In other words, all methods fall short of magnitude pruning after training. Considering this fact, our approach avoids multiple rounds of training and finds a sparse structure in one single round of training. Additionally, sparsity is forced during the training process and not afterwards.

3 Finding a sparse trainable network

3.1 Problem explanation

Finding a sparse network whose accuracy is on a par with a dense network amounts to solving a bi-level, constrained, stochastic, nonconvex, and non-smooth sparse optimization problem as follows:

$$\boldsymbol{\theta}^* = \left\{ \begin{array}{l} \arg \min_{\hat{\boldsymbol{\theta}}} \|\hat{\boldsymbol{\theta}}\|_0 \\ \text{s.t. } \hat{\boldsymbol{\theta}} = \arg \min_{\boldsymbol{\theta}} \mathbb{E}_{\mathbf{x} \sim \mathcal{D}} [f(\mathbf{y}(\mathbf{x}), \mathbf{h}(\mathbf{x}; \boldsymbol{\theta}))] \end{array} \right\}. \quad (1)$$

where $\mathbf{h}(\mathbf{x}; \boldsymbol{\theta})$ is the vector-valued neural network function whose input is a random vector $\mathbf{x} \sim \mathcal{D}$ labeled by random vector $\mathbf{y}(\mathbf{x})$ and its parameters are denoted by $\boldsymbol{\theta} \in \mathbb{R}^d$. The scalar-valued function f is the cost or loss function, also known as the criterion, $\|\boldsymbol{\theta}\|_0$ is the number of nonzero elements of $\boldsymbol{\theta}$, or the ℓ_0 norm¹. In Problem (1): having two optimizations simultaneously makes it bi-level, \mathcal{D} is the source of stochasticity and is unknown, composition of f and \mathbf{h} make the objective function nonconvex, and since ℓ_0 norm is not differentiable, one deals with a non-smooth problem. If one can solve Problem (1), the energy consumption reduces, hardware requirements are relaxed, and performing inference become faster. Unfortunately, even a deterministic and convex sparse optimization problem, e.g., least-squares problem, is a combinatorial and NP-hard problem (Davis and Mallat, 1994; Natarajan, 1995). Therefore, the best approach is to convert the current bi-level optimization problem into another optimization problem that is neither bi-level, stochastic, nor non-smooth. Solving the new optimization problem will find an approximate solution to the original Problem (1), i.e., $\hat{\boldsymbol{\theta}}^*$. However, the unanswered question is how to convert Problem (1) to a solvable approximate problem. By trial and error, one can find an upper bound for the sparsity of the vector parameter, i.e., $\|\boldsymbol{\theta}^*\|_0 \lesssim \hat{s}$. Given the sparsity level \hat{s} , we get the following optimization problem:

$$(\tilde{\boldsymbol{\theta}}^* \odot \tilde{\mathbf{m}}^*) = \left\{ \arg \min_{\boldsymbol{\theta}, \mathbf{m}} \mathbb{E}_{\mathbf{x} \sim \mathcal{D}} [f(\mathbf{y}(\mathbf{x}), \mathbf{h}(\mathbf{x}; \boldsymbol{\theta} \odot \mathbf{m}))] \quad \text{s.t. } \|\mathbf{m}\|_0 \leq \hat{s} \right\}, \quad (2)$$

where $\mathbf{m} = \{0, 1\}^d$ is a binary mask and \odot denotes Hadamard product operator. Unlike Problem (1) where a sparsity level is automatically found, i.e., s^* , here sparsity level \hat{s} is given. Because of this fact, solutions to Problem (1) and (2), that are $\boldsymbol{\theta}^*$ and $\tilde{\boldsymbol{\theta}}^* \odot \tilde{\mathbf{m}}^*$, may not be the same. Having an accurate estimate for $\hat{s} \gtrsim s^*$ relaxes Problem (1) from being a bi-level optimization problem to a single level problem. However, all the other issues mentioned above still stay with Problem (2). Now from the perspective of optimization, the first question would be whether this problem is feasible or not. Empirically, Frankle and Carbin (2018) addressed this problem for the first time and conjectured that such a solution exists and named their conjecture the *lottery ticket hypothesis*. Mathematically speaking, the *lottery ticket hypothesis* conjectures that Problem (2) for $\hat{s} \gtrsim s^*$ is feasible and there exists a solution to that.

Once we know the solution exists, the most straightforward approach to find an approximate solution to Problem (2) is to first find a mask $\hat{\mathbf{m}}$ which is a good estimate of $\tilde{\mathbf{m}}^*$. To estimate $\hat{\mathbf{m}}$, there are two extreme approaches. One approach finds $\hat{\mathbf{m}}$ using multiple rounds of training (Frankle and Carbin,

¹ ℓ_0 is not mathematically a norm because for any norm $\|\cdot\|$ and $\alpha \in \mathbb{R}$, $\|\alpha\boldsymbol{\theta}\| = |\alpha|\|\boldsymbol{\theta}\|$, while $\|\alpha\boldsymbol{\theta}\|_0 = |\alpha|\|\boldsymbol{\theta}\|_0$ if and only if $|\alpha| = 1$

2018; Frankle et al., 2019; Savarese et al., 2019), and the other finds it at the beginning of training (Lee et al., 2018; Wang et al., 2020; Tanaka et al., 2020). As opposed to the latter, the former reaches test accuracy of the dense network (Gale et al., 2019; Frankle et al., 2020), but it is computationally expensive. Once an accurate mask, i.e., $\hat{\mathbf{m}} \approx \tilde{\mathbf{m}}^*$ is at hand, the non-smoothness and constraint of Problem (2) can be relaxed. Also, by assuming large sample size and using stochastic approximation of the expected value in the objective function (Ghadimi and Lan, 2013), one can use the following unconstrained optimization problem as a relaxation for Problem (2):

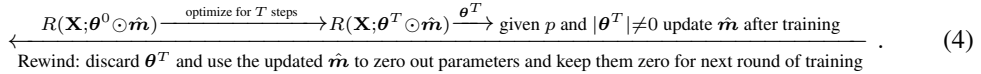
$$(\hat{\boldsymbol{\theta}}^* \odot \hat{\mathbf{m}}) \approx \arg \min_{\boldsymbol{\theta}} R(\mathbf{X}; \boldsymbol{\theta} \odot \hat{\mathbf{m}}) \approx \arg \min_{\boldsymbol{\theta}} \mathbb{E}_{\mathbf{x} \sim \mathcal{D}} \left[f(\mathbf{y}(\mathbf{x}), \mathbf{h}(\mathbf{x}; \boldsymbol{\theta} \odot \hat{\mathbf{m}})) \right], \quad (3)$$

where $R(\mathbf{X}; \boldsymbol{\theta} \odot \hat{\mathbf{m}}) = M^{-1} \sum_{i=1}^M f(\mathbf{y}(\mathbf{x}^{(i)}), \mathbf{h}(\mathbf{x}^{(i)}; \boldsymbol{\theta} \odot \hat{\mathbf{m}}))$, $\mathbf{X} = [\mathbf{x}^{(1)}, \dots, \mathbf{x}^{(M)}]$ is the data matrix, $\mathbf{x}^{(i)}$ for $i = 1, \dots, M$ is a realization of $\mathbf{x} \sim \mathcal{D}$, and $\mathbf{y}(\mathbf{x}^{(i)})$ is the realized target associated with $\mathbf{x}^{(i)}$.

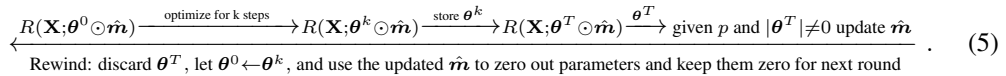
3.2 Acceptable initialization

As far as solving Problem (3) is concerned, given an accurate $\hat{\mathbf{m}}$, every initialization that can converge to a solution would be acceptable, which is why Frankle and Carbin (2018) use the original initialization but Frankle et al. (2019) use parameters from the k -th step of each optimization round. The following discussion will make this point more clear.

The first version of *the lottery ticket algorithm* proposes Scheme (4) that solves Problem (3) for r rounds when $\hat{\mathbf{m}}$ is assumed to be given. In order to find a sparse network, Scheme (4) starts from $\hat{\mathbf{m}} = \mathbf{1}$ and updates it at the end of each round as follows:



At the end of each round $\hat{\mathbf{m}}$ gets updated by zeroing out $p\%$ of nonzero entries in it. However, Scheme (4) fails to find the ticket for large networks such as ResNet50. This can be solved by the following scheme proposed by Frankle et al. (2019) which starts from $\hat{\mathbf{m}} = \mathbf{1}$:



There are a couple of observations that should be made here. Firstly, Scheme (5) changes the definition of the *lottery ticket* to a sparse network with sparse initialization coming from the k -th step of the optimization. This modification is useful since a sparse neighborhood of $\boldsymbol{\theta}^0$ which is a small neighborhood in a lower dimensional space with dimension $\|\hat{\mathbf{m}}\|_0$ cannot be a good initialization, so the optimization algorithm cannot converge to the test loss of the dense network. However, a sparse neighborhood of $\boldsymbol{\theta}^k$ provides a point from which convergence is guaranteed. That is, $\|\hat{\boldsymbol{\theta}}^* \odot \hat{\mathbf{m}} - \boldsymbol{\theta}^k \odot \hat{\mathbf{m}}\|_2$ is smaller than $\|\hat{\boldsymbol{\theta}}^* \odot \hat{\mathbf{m}} - \boldsymbol{\theta}^0 \odot \hat{\mathbf{m}}\|_2$, which means $\boldsymbol{\theta}^k \odot \hat{\mathbf{m}}$ is closer to $\hat{\boldsymbol{\theta}}^* \odot \hat{\mathbf{m}}$ than $\boldsymbol{\theta}^0 \odot \hat{\mathbf{m}}$. Secondly, one careful observer may argue that parameter values at the k -th step, i.e., $\boldsymbol{\theta}^k \odot \hat{\mathbf{m}}$, are stochastic values since an SGD-style algorithm is stochastic by its nature. Hence, starting from a fixed initialization, $\boldsymbol{\theta}^0 \odot \hat{\mathbf{m}}$, does not guarantee to have the same values for the parameters at step k . That being said, the lottery ticket can be any sparse network with any sparse initialization that can reach the test accuracy of the dense network. This is equivalent to saying that every initialization from which Problem (3) can be solved iteratively is an acceptable initialization. In this sense, we will propose an algorithm that finds a mask $\hat{\mathbf{m}}$ together with an acceptable initialization from which an iterative algorithm can solve Problem (3).

3.3 Amenable Sparse Network Investigator algorithm

We present the ‘‘Amenable Sparse Network Investigator’’ (ASNI) algorithm. ASNI first learns a trained sparse structure. This learned sparse structure is trainable. Its trainability depends on L pairs of signed centroids that are sufficient to initialize the learned sparse structure. Being able to be trained from a compressed set of initialization, makes the learned sparse network ‘‘amenable’’. As Figure (1) shows, after pruning the dense network by ASNI, each layer l has a pair of signed centroids (positive and negative), i.e., $\bar{\mathbf{c}}_+^{[l]}, \bar{\mathbf{c}}_-^{[l]}$, which are means of two distinct normal-like distributions. Once they are replaced instead of positive and negative learned values, the sparse network is trainable and reaches virtually the nominal test accuracy of the dense network.

3.4 ASNI anatomy

ASNI algorithm follows a simple intuitive and easy to implement strategy for determining the overall sparsity percentage not layer-wise. ASNI determines sparsity percentage by utilizing a sigmoid function as $p = \alpha \text{ sigmoid}((e - \beta E)/\gamma)$ for $e = 1, \dots, E$, where E is the total number of epochs, α controls the final sparsity, β governs how early and late pruning starts and stops, and γ controls how fast pruning should be done. Figure (2a) shows two different realizations of the overall percentage for different scenarios. This sparsity strategy can allow the network to learn the main structure at the early stages of pruning. As an example for the case $\beta = 10$ in Figure (2a), this strategy lets the network learn with full capacity up to 5-th epoch. Until then the network sparsity has to be very small. This helps the algorithm fall into a good neighborhood surrounding a local minimum as we discussed in Section (3.2). After that, it tries to correct mistakes very gently by zeroing out nonzero parameters that are not important. This happens with a small slope until almost epoch 35. Once it makes sure that the network has learned the main structure, the slope increases until epoch 60. From that point on, the sparsity percentage decreases to recover from all the previous pruning in order to reach the maximum allowed sparsity level. Once sparsity percentage is determined at Line 5 of Alg. (1), ASNI prunes nonzero parameters of the network with respect to a global pruning threshold, i.e., $\tau_g > 0$, which is obtained after each epoch of training according to Line 6. The global threshold is calculated by gathering magnitudes of all parameters except the bias and batch normalization parameters, since the number of these parameters is negligible. $\tau_g > 0$ is found such that the magnitude of $p\%$ of all gathered parameters are less than τ_g , and $(100 - p)\%$ are above the global threshold. Next, ASNI zeros out the entries of the mask vector for those parameters whose magnitudes are less than τ_g (Line 7)². This is where the mask vector $\hat{\mathbf{m}}$ gets updated. Once ASNI updates the mask, retraining restarts for another epoch. As the last epoch finishes, the vector of parameters would be the learned sparse vector, i.e., $\hat{\boldsymbol{\theta}}^*$ which is a sparse approximate solution to Problem (2) and $\hat{\mathbf{m}}$ identifies the learned sparse structure. Once $\hat{\boldsymbol{\theta}}^*$ is found, centroids ($\bar{\mathbf{c}}_+^{[l]}, \bar{\mathbf{c}}_-^{[l]}$) are calculated accordingly based on Lines 12-18 where ASNI takes the average of positive and negative parameters separately. Note that initialization for batch normalization weights is one and initialization for biases is zero.

Algorithm 1 The ASNI algorithm

Require: Initial parameter vector $\boldsymbol{\theta}^0$, training data \mathbf{X}_{tr} , epochs E , optimizer's parameters, e.g., initial learning rate $\eta = \eta_0$, cosine scale δ , mini-batch size b , initial mask vector $\hat{\mathbf{m}} = \mathbf{1}$, sigmoid's parameters α, β, γ .

- 1: **for** $e = 1$ to E **do**
- 2: **for** $k = 1$ to T **do**
- 3: $\boldsymbol{\theta}^k \leftarrow \boldsymbol{\theta}^{k-1} - \eta (\nabla R(\mathbf{X}_{tr,b}; \boldsymbol{\theta}^{k-1})) \odot \hat{\mathbf{m}}$
- 4: **end for**
- 5: $p = \alpha \text{ sigmoid}((e - \beta E)/\gamma)$
- 6: $\tau_g = p\text{-th percentile of } \{|\boldsymbol{\theta}|\}$
- 7: $\hat{\mathbf{m}} = \mathbf{1}_{|s| \geq \tau_g}(|\mathbf{s}|)$
- 8: $\eta = \eta_0 \cos(\pi e / (1 + \delta)E)$
- 9: $\boldsymbol{\theta}^0 \leftarrow \boldsymbol{\theta}^T \odot \hat{\mathbf{m}}$
- 10: **end for**

- 11: $\hat{\boldsymbol{\theta}}^* \leftarrow \boldsymbol{\theta}^0$
- 12: **for** $l = 1$ to L **do**
- 13: $\bar{\mathbf{c}}_+^{[l]} = \text{mean}(\hat{\boldsymbol{\theta}}^*_{+}^{[l]} > 0)$
- 14: $\boldsymbol{\theta}^{[l]}_+ = \bar{\mathbf{c}}_+^{[l]} \mathbf{1}_{\hat{\boldsymbol{\theta}}^*_{+}^{[l]} > 0}(\hat{\boldsymbol{\theta}}^*_{+}^{[l]})$
- 15: $\bar{\mathbf{c}}_-^{[l]} = \text{mean}(\hat{\boldsymbol{\theta}}^*_{-}^{[l]} < 0)$
- 16: $\boldsymbol{\theta}^{[l]}_- = \bar{\mathbf{c}}_-^{[l]} \mathbf{1}_{\hat{\boldsymbol{\theta}}^*_{-}^{[l]} < 0}(\hat{\boldsymbol{\theta}}^*_{-}^{[l]})$
- 17: $\boldsymbol{\theta}^{[l]}_0 = \boldsymbol{\theta}^{[l]}_- + \boldsymbol{\theta}^{[l]}_+$
- 18: **end for**
- 19: **Output:** $\hat{\boldsymbol{\theta}}^*, \boldsymbol{\theta}^0, \bar{\mathbf{c}}_+, \bar{\mathbf{c}}_-$ and $\hat{\mathbf{m}}$

² $\mathbf{1}_A(x) = \{1 \text{ if } x \in A, 0 \text{ if } x \notin A\}$

4 Experiments

This section explains the setup of our experiments. Due to the large number of experiments, some results have been moved to Appendix B for the sake of clarity and completeness. Table 1 summarizes combination of datasets and networks, number of trainable parameters, number of epochs of training, mini-batch size, optimizer, the initial learning rate, and learning rate policy.

Table 1: Combination of datasets and networks with their hyper parameters.

Dataset	Network	Params	Epochs	Batch Size	Opt.	LR policy	LR/WD	δ	Iters/epoch
MNIST	FC	266,610	50	60	Adam	Constant	1.2e-3	—	1000
MNIST	Conv2	3,317,450	20	60	Adam	Constant	2e-4	—	1000
MNIST	Conv4	1,933,258	25	60	Adam	Constant	3e-4	—	1000
MNIST	Conv6	1,802,698	30	60	Adam	Constant	3e-4	—	1000
CIFAR-10	Conv2	4,301,642	20	60	Adam	Constant	2e-4	—	1000
CIFAR-10	Conv4	2,425,930	25	60	Adam	Constant	3e-4	—	1000
CIFAR-10	Conv6	2,262,602	30	60	Adam	Constant	3e-4	—	1000
CIFAR-10	VGG-11	9,231,114	160	128	SGD+M	cosine	0.05/5e-4	0.06	391
CIFAR-10	VGG-13	9,416,010	160	128	SGD+M	cosine	0.05/5e-4	0.06	391
CIFAR-10	VGG-16	14,728,266	160	128	SGD+M	cosine	0.05/5e-4	0.06	391
CIFAR-10	ResNet-18	11,181,642	160	128	SGD+M	cosine	0.05/5e-4	0.06	391
ImageNet	ResNet-50	25,557,032	90	820	SGD+M	cosine	0.35/1e-4	0.02	6252

4.1 Setup

Our experiments involve image classification on well-known datasets including the MNIST (LeCun, 1998), CIFAR-10 (Krizhevsky et al., 2009), and the ImageNet-1K (Russakovsky et al., 2015).

Network architectures that we utilize include the 3-layer fully-connected network (LeNet-300-100) (LeCun et al., 1998) named FC, convolutional neural networks (CNNs), named Conv-2, Conv-4, and Conv-6 (small CNNs with 2/4/6 convolutional layers, same as in (Frankle and Carbin, 2018)). We also use ResNet-18/34/50 (He et al., 2016). Additionally, we utilize VGG-style networks (Simonyan and Zisserman, 2014) named as VGG-11/13/16/19 with batch normalization and an average pooling after convolution layers followed by a fully connected layer. As a result of the average pooling, parameter count of these VGG-style networks decreases which mitigates the parameter inefficiency with original VGG networks.

We use stochastic gradient descent (Robbins and Monroe, 1951) with momentum (Nesterov, 1983) (SGD+M), or Adam (Kingma and Ba, 2014) as our optimizers. We set the momentum coefficient for all experiments to 0.9 when SGD+M is used. For cases where learning rate follows a cosine policy, cosine learning rate is defined as $\eta = \eta_0 \cos(\pi e / (1 + \delta) E)$ where η_0 is the initial learning rate, E is the total number of epochs, and nonzero δ controls the final learning rate. For ImageNet-1K our training pipeline uses standard data augmentation, which includes random flips and crops. Network parameters are initialized according to the Kaiming Normal distribution (He et al., 2015).

For all experiments we use Pytorch (Paszke et al., 2019) and for training we use native PyTorch automatic mixed precision (AMP) to boost the speed of training. Networks are trained using NVIDIA TITAN X (Pascal) 12GB GPUs.

4.2 Results

Table 2 shows pruning hyper parameters and test accuracy of every experiments that considers four variants. Each test accuracy of four accuracies in a row is an average of 3 different runs.

4.2.1 Network parameters distribution

The ASNI algorithm uses a global threshold that considers every parameter in all layers. Therefore, it makes sense to look at the distribution of all parameters at once and not in layer-wise fashion. We do this for the ResNet-50 network trained on ImageNet-1K. Similar distributions can be found in Appendix B. As Figure (3) shows, initial parameters (orange) have the largest variance. On the other hand, distribution of the learned parameters of a dense network (red) has so many small values. This makes sense since having so many parameters lets the optimization algorithm have the ability to

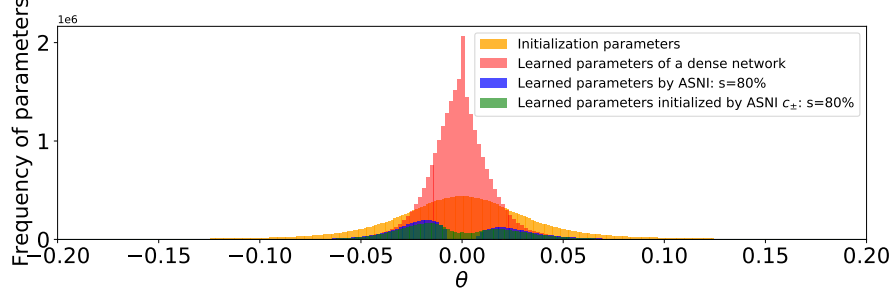


Figure 3: Parameter distribution considering all parameters in every layer of a ResNet-50 network trained on ImageNet-1K: the orange plot shows distribution of the dense network initialization, the red plot is the distribution of learned parameters when the network is dense, the blue one is the distribution of parameters learned by *ASNI* at $s \approx 80\%$, and the distribution of parameters for learned sparse network ($s \approx 80\%$) initialized by centroids. Dense initialization (orange) covers the widest range of values while the learned parameters for the dense network (red) have the shortest range. Parameters learned by *ASNI* (blue) are two distinct normal-like distributions where parameters with small absolute values are discarded. Distribution of the learned parameters (green) initialized by centroids looks like the sum of two normal distributions whose means coincide with centroids.

change each parameter a little bit to find a local minimum. Distribution of parameters learned by *ASNI* (blue) is two normal-like distributions where small values (in absolute value sense) has been discarded. Ignoring small values is what *ASNI* forces but observing two truncated normal-like distribution is surprising. The more surprising phenomenon is the distribution of the learned parameters of the learned sparse structure that is initialized by learned centroids (green). This distribution covers the distribution of parameters learned by *ASNI* and fills the gap between them. This means that the learned sparse structure initialized by centroids is also able to learn the learned parameters by *ASNI*.

If we look at distribution of the parameters learned by *ASNI* at each layer similar to what is shown in Figure (1), one can observe that we not only have two normal-like distributions for all parameters, but also have this pattern for each layer. That motivated us to use means of positive and negative values learned by *ASNI* to initialize the network.

4.3 Test accuracy

As Figure (2b) indicates and Table 2 shows precisely, the learned sparse network (blue) and the sparse structure initialized by the learned centroids (green) reach test accuracy of the dense network (red) but the learned sparse structure initialized by the original initialization (orange) falls short of the other ones. Note that, there are two important considerations that should be taken care of. First, *ASNI* is able to generate sparse accurate ResNet-50 since it uses cosine learning rate. It does not reach test accuracy of the dense network with discrete learning rate which is decayed by a factor of two or ten during the training. This is because *ASNI* prunes gradually so its learning rate should be adjusted accordingly. Another important point for ResNet-50 is that learned sparse networks should be trained with smaller learning rate (0.128) than the original one. By utilizing the smaller learning rate we can train the learned sparse network initialized by centroids to reach the accuracy of the dense network.

In Table 2 dense accuracy is not always the highest and sometimes *ASNI* perform better even if it has far less parameters than the dense one. Another pattern in Table 2 is that networks initialized by the original initialization cannot reach test accuracy that the compressed initialization can reach. Notably, both of the network trained with sparse initialization perform well which means the mask learned by *ASNI* is a very good mask.

4.4 Sparsity distribution

ASNI prunes parameters of the network to reach a predefined sparsity percentage. After reaching sparsity value the question is which layers have been pruned more and which layers still are denser than others. As *ASNI* does not enforce any limitations on the sparsity of layers, each one can be pruned differently. According to Figure (4) layers are pruned non-uniformly. Among them the last layer (black) which is a fully connected one is pruned less. The first convolutional layer outside of stages (black) is the second one with least pruning. When one looks at the stages, one can figure out

Table 2: Hyper parameters for pruning and test accuracy of four variants. Top-1 is the average of 3 test accuracies. (Top-1D): dense network with zero sparsity, (Top-1A): trained with *ASNI* that has sparsity given in Column 6, (Top-1C) the learned sparse network reinitialized by *ASNI* initialization (c_{\pm}), and (Top-1S) the learned sparse network reinitialized by the original initialization.

Dataset	Network	α	β	γ	Sparsity%	Nonzeros	Top-1D%	Top-1A%	Top-1C%	Top-1S%
MNIST	FC	98	0.5	5	96.87	8,335	96.88	96.72	96.93	96.75
MNIST	Conv2	99.2	0.5	2	98.18	86,363	98.09	98.12	98.14	98.03
MNIST	Conv4	98.5	0.5	2	97.94	39,828	98.33	98.46	98.52	98.27
MNIST	Conv6	98.5	0.5	3	97.15	51,420	98.25	98.54	98.53	98.36
CIFAR-10	Conv2	98.5	0.5	2	96.71	141,364	76.10	74.61	76.4	75.26
CIFAR-10	Conv4	95	0.5	2	94.47	134,185	84.34	84	83.76	83.24
CIFAR-10	Conv6	94	0.5	3	92.72	164,624	86.69	86.1	85.72	85.55
CIFAR-10	VGG-11	97	0.5	16	96.14	356,230	92.40	91.51	91.18	89.94
CIFAR-10	VGG-13	98	0.5	16	97.14	269,221	94.23	92.98	92.29	91.67
CIFAR-10	VGG-16	99	0.5	16	98.15	272,626	93.90	93.45	92.13	91.94
CIFAR-10	ResNet-18	97	0.5	16	96.14	451,216	88.24	87.78	87.32	87.15
ImageNet	ResNet-50	81.04	0.5	10	80.12	5,140,882	75.02	74.58	74.78	69.89
ImageNet	ResNet-50	91.05	0.5	10	90.08	2,534,267	75.02	73.18	72.79	65.43

the first convolutional layer in the first bottleneck of each stage is the layer with the least pruning. Surprisingly, the last bottleneck of first and last stages are similar in a sense that they are sparsified less than other bottlenecks.

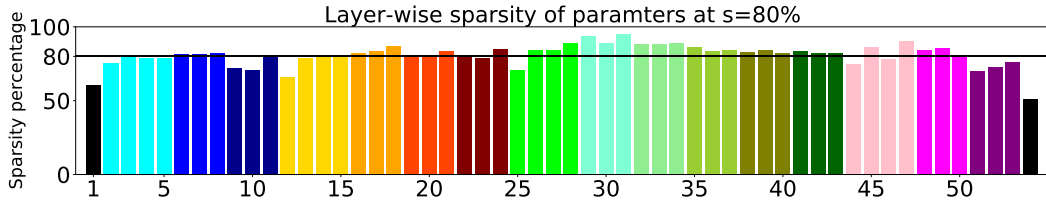


Figure 4: Layer-wise sparsity after training a ResNet-50 network. The network has 4 main stages where stages have 3, 4, 6, and 3 bottlenecks respectively. The stages are color-coded with blue (2-11), red (12-24), green (25-43), and pink (44-53). Black bars are sparsity percentage of the first convolution layer (not in stages) and the fully connected layer at the end. Each first convolution layer in a stage which is in the first bottleneck of the stage is hatched with lines and the skip connection of the stage is hatched with stars. The least sparsity occurs at the last layer (54) which is a fully connected one. Also, first convolution layers (2, 12, 25, 44) in the first bottleneck of each stage are the ones with the smallest sparsity compared to other convolutional layers in stages.

5 Conclusion and discussion

We proposed the *ASNI* algorithm that avoids multiple round search for finding a sparse trainable structure. The learned sparse structure together with its compressed initialization set can reach test accuracy of the dense network and is superior over the masks learned before training. By utilizing the fact that early stages of pruning are important and the network learns the structure in these stages (Achille et al., 2018; Frankle et al., 2019; You et al., 2019), a sigmoid function was proposed to control the sparsity at early stages as well as every epoch of one single training round. Furthermore, we noticed that the amount of pruning at each round makes a difference, since after each round of pruning we have a new sparse network that should be treated differently. Therefore, the pruning percentage of each sparse network at each round should be different.

References

- Achille, A., Rovere, M., and Soatto, S. (2018). Critical learning periods in deep networks. In *International Conference on Learning Representations*.
- Davis, G. and Mallat, S. (1994). *Adaptive nonlinear approximations*. PhD thesis, New York University, Graduate School of Arts and Science.
- Denil, M., Shakibi, B., Dinh, L., Ranzato, M., and De Freitas, N. (2013). Predicting parameters in deep learning. In *Advances in neural info. processing systems*, pages 2148–2156.
- Dettmers, T. and Zettlemoyer, L. (2019). Sparse networks from scratch: Faster training without losing performance. *arXiv preprint arXiv:1907.04840*.
- Evcı, U., Gale, T., Menick, J., Castro, P. S., and Elsen, E. (2020). Rigging the lottery: Making all tickets winners. In *International Conference on Machine Learning*, pages 2943–2952. PMLR.
- Frankle, J. and Carbin, M. (2018). The lottery ticket hypothesis: Finding sparse, trainable neural networks. *arXiv preprint arXiv:1803.03635*.
- Frankle, J., Dziugaite, G. K., Roy, D. M., and Carbin, M. (2019). Stabilizing the lottery ticket hypothesis. *arXiv preprint arXiv:1903.01611*.
- Frankle, J., Dziugaite, G. K., Roy, D. M., and Carbin, M. (2020). Pruning neural networks at initialization: Why are we missing the mark? *arXiv preprint arXiv:2009.08576*.
- Gale, T., Elsen, E., and Hooker, S. (2019). The state of sparsity in deep neural networks. *arXiv preprint arXiv:1902.09574*.
- Ghadimi, S. and Lan, G. (2013). Stochastic first-and zeroth-order methods for nonconvex stochastic programming. *SIAM Journal on Optimization*, 23(4):2341–2368.
- Guo, Y., Yao, A., and Chen, Y. (2016). Dynamic network surgery for efficient dnns. *arXiv preprint arXiv:1608.04493*.
- Han, S., Mao, H., and Dally, W. J. (2015a). Deep compression: Compressing deep neural networks with pruning, trained quantization and huffman coding. *arXiv preprint arXiv:1510.00149*.
- Han, S., Pool, J., Tran, J., and Dally, W. (2015b). Learning both weights and connections for efficient neural network. In *Advances in neural info. processing systems*, pages 1135–1143.
- Hanson, S. J. and Pratt, L. Y. (1989). Comparing biases for minimal network construction with back-propagation. In *Advances in neural info. processing systems*, pages 177–185.
- Hassibi, B. and Stork, D. G. (1993). Second order derivatives for network pruning: Optimal brain surgeon. In *Advances in neural information processing systems*, pages 164–171.
- He, K., Zhang, X., Ren, S., and Sun, J. (2015). Delving deep into rectifiers: Surpassing human-level performance on imagenet classification. In *Proceedings of the IEEE international conference on computer vision*, pages 1026–1034.
- He, K., Zhang, X., Ren, S., and Sun, J. (2016). Deep residual learning for image recognition. In *Proceedings of the IEEE conference on computer vision and pattern recognition*, pages 770–778.
- Kingma, D. P. and Ba, J. (2014). Adam: A method for stochastic optimization. *arXiv preprint arXiv:1412.6980*.
- Krizhevsky, A., Nair, V., and Hinton, G. (2009). Cifar-10 and cifar-100 datasets. URL: <https://www.cs.toronto.edu/kriz/cifar.html>, 6(1):1.
- Kusupati, A., Ramanujan, V., Somani, R., Wortsman, M., Jain, P., Kakade, S., and Farhadi, A. (2020). Soft threshold weight reparameterization for learnable sparsity. *arXiv preprint arXiv:2002.03231*.
- LeCun, Y. (1998). The mnist database of handwritten digits. <http://yann.lecun.com/exdb/mnist/>.

- LeCun, Y., Bottou, L., Bengio, Y., and Haffner, P. (1998). Gradient-based learning applied to document recognition. *Proceedings of the IEEE*, 86(11):2278–2324.
- LeCun, Y., Denker, J. S., and Solla, S. A. (1990). Optimal brain damage. In *Advances in neural information processing systems*, pages 598–605.
- Lee, N., Ajanthan, T., and Torr, P. H. (2018). Snip: Single-shot network pruning based on connection sensitivity. *arXiv preprint arXiv:1810.02340*.
- Li, H., Kadav, A., Durdanovic, I., Samet, H., and Graf, H. P. (2016). Pruning filters for efficient convnets. *arXiv preprint arXiv:1608.08710*.
- Liu, Z., Sun, M., Zhou, T., Huang, G., and Darrell, T. (2018). Rethinking the value of network pruning. *arXiv preprint arXiv:1810.05270*.
- Louizos, C., Welling, M., and Kingma, D. P. (2017). Learning sparse neural networks through l_0 regularization. *arXiv preprint arXiv:1712.01312*.
- Luo, J.-H., Wu, J., and Lin, W. (2017). Thinet: A filter level pruning method for deep neural network compression. In *Proceedings of the IEEE international conference on computer vision*, pages 5058–5066.
- Mocanu, D. C., Mocanu, E., Stone, P., Nguyen, P. H., Gibescu, M., and Liotta, A. (2018). Scalable training of artificial neural networks with adaptive sparse connectivity inspired by network science. *Nature communications*, 9(1):1–12.
- Molchanov, P., Tyree, S., Karras, T., Aila, T., and Kautz, J. (2016). Pruning convolutional neural networks for resource efficient inference. *arXiv preprint arXiv:1611.06440*.
- Mostafa, H. and Wang, X. (2019). Parameter efficient training of deep convolutional neural networks by dynamic sparse reparameterization. In *International Conference on Machine Learning*, pages 4646–4655. PMLR.
- Narang, S., Elsen, E., Diamos, G., and Sengupta, S. (2017). Exploring sparsity in recurrent neural networks. *arXiv preprint arXiv:1704.05119*.
- Natarajan, B. K. (1995). Sparse approximate solutions to linear systems. *SIAM journal on computing*, 24(2):227–234.
- Nesterov, Y. E. (1983). A method for solving the convex programming problem with convergence rate $O(1/k^2)$. In *Dokl. akad. nauk Sssr*, volume 269, pages 543–547.
- Paszke, A., Gross, S., Massa, F., Lerer, A., Bradbury, J., Chanan, G., Killeen, T., Lin, Z., Gimelshein, N., Antiga, L., et al. (2019). Pytorch: An imperative style, high-performance deep learning library. *arXiv preprint arXiv:1912.01703*.
- Robbins, H. and Monro, S. (1951). A stochastic approximation method. *The annals of mathematical statistics*, pages 400–407.
- Russakovsky, O., Deng, J., Su, H., Krause, J., Satheesh, S., Ma, S., Huang, Z., Karpathy, A., Khosla, A., Bernstein, M., et al. (2015). Imagenet large scale visual recognition challenge. *International journal of computer vision*, 115(3):211–252.
- Savarese, P., Silva, H., and Maire, M. (2019). Winning the lottery with continuous sparsification. *arXiv preprint arXiv:1912.04427*.
- Simonyan, K. and Zisserman, A. (2014). Very deep convolutional networks for large-scale image recognition. *arXiv preprint arXiv:1409.1556*.
- Tanaka, H., Kunin, D., Yamins, D. L., and Ganguli, S. (2020). Pruning neural networks without any data by iteratively conserving synaptic flow. *arXiv preprint arXiv:2006.05467*.
- Tartaglione, E., Lepsøy, S., Fiandrötti, A., and Francini, G. (2018). Learning sparse neural networks via sensitivity-driven regularization. *arXiv preprint arXiv:1810.11764*.

- Wang, C., Zhang, G., and Grosse, R. (2020). Picking winning tickets before training by preserving gradient flow. *arXiv preprint arXiv:2002.07376*.
- Wen, W., Wu, C., Wang, Y., Chen, Y., and Li, H. (2016). Learning structured sparsity in deep neural networks. *arXiv preprint arXiv:1608.03665*.
- You, H., Li, C., Xu, P., Fu, Y., Wang, Y., Chen, X., Baraniuk, R. G., Wang, Z., and Lin, Y. (2019). Drawing early-bird tickets: Towards more efficient training of deep networks. *arXiv preprint arXiv:1909.11957*.
- Zhu, M. and Gupta, S. (2017). To prune, or not to prune: exploring the efficacy of pruning for model compression. *arXiv preprint arXiv:1710.01878*.

A Appendix

A.1 Foresight pruning

In this section we will go over methods that try to resolve the first issue, which is solving optimization Problem (3) for multiple rounds. These algorithms try to train a sparse structure initialized by $\theta^0 \odot \hat{m}$ with $\|\hat{m}\|_0 \ll d$ before training. To this end, Lee et al. (2018) was the first work posited the idea of foresight pruning (pruning at the initialization) which is performed as a single shot of pruning. In this approach (SNIP), a *connection sensitivity* score is calculated as $s = \theta^0 \odot \nabla_{\theta} R(\mathbf{X}; \theta^0)$ before training. See Appendix A.1.1 for different derivations of s and the intuition behind it. Then a fixed mask will be generated using the obtained *connection sensitivity* vector as $\hat{m} = \mathbf{1}_{|s_j| \geq \tau_k}(|s|)$ ³ where τ_k is the k -th top entry of $|s|$ and $j = 1, \dots, d$. Once the mask is acquired it solves Problem (3). There are two downsides with SNIP. The first issue is that the absolute value of *connection sensitivity* score promotes entries whose absolute values or their gradients are large or both. However, the goal is to keep entries whose gradients are large before training since those are the ones that are most sensitive. Unfortunately, $|s|$ does not provide information in this manner. The second issue will be addressed later.

Since *connection sensitivity* score has its own flaws, others have tried to find better scoring vectors. For example Wang et al. (2020) introduce GraSP, utilizing Hessian-gradient product, i.e., \mathbf{Hg} , which leads to $s = -\theta^0 \odot \mathbf{Hg}(\theta^0)$. This score can also be used as a tool for removing parameters. See Appendix A.1.2 for derivation of s and read more about its soundness. Along the same direction, we can also mention (Tanaka et al., 2020) that finds the mask before training.

Now, we can get back to the second issue of SNIP which is an issue with the last two other algorithms. The performance of these methods that apply pruning before training is not competitive with performance of networks whose initializations are obtained using pruning far later in training (Gale et al., 2019; Frankle et al., 2020). In other words, all methods fall short of magnitude pruning after training. One answer may be is that they all calculate s using the stochastic gradient which is an estimation of the true gradient and is calculated for a random single mini-batch of data (Appendices A.1.1 and A.1.2 show how these score are obtained from the true gradient at initialization). This estimation may be drastically dissimilar to another stochastic gradient that uses a different mini-batch.

A.1.1 Connection sensitivity score

Reparameterize $R(\mathbf{X}; \theta)$ with $\mathbf{c} \in \mathbb{R}^d$ to get $R(\mathbf{X}; \theta \odot \mathbf{c})$. The ultimate goal is to find the gradient of $R(\mathbf{X}; \theta \odot \mathbf{c})$ with respect to \mathbf{c} and evaluate it when $\mathbf{c} = \mathbf{1}$, i.e., $\nabla_{\mathbf{c}} R(\mathbf{X}; \theta \odot \mathbf{c})|_{\mathbf{c}=\mathbf{1}}$. The Hadamard product $\theta \odot \mathbf{c}$ can be written as a matrix product, i.e., $\text{diag}(\mathbf{c})\theta$. Let $\mathbf{A}(\mathbf{c}) = \text{diag}(\mathbf{c})$ be a matrix-valued function of \mathbf{c} . Hence, one can write $g(\theta, \mathbf{c}) = R(\mathbf{X}; \mathbf{A}(\mathbf{c})\theta)$. The gradient of scalar-valued function $g(\theta, \mathbf{c})$ can be written in terms of the Jacobian matrix as $\nabla_{\mathbf{c}}^T g(\theta, \mathbf{c}) = J_{\mathbf{c}} g(\theta, \mathbf{c}) = J_{\mathbf{c}} R(\mathbf{X}; \mathbf{A}(\mathbf{c})\theta)$. Using the chain rule one can write the following:

$$\begin{aligned} \nabla_{\mathbf{c}}^T g(\theta, \mathbf{c}) &= J_{\mathbf{c}} R(\mathbf{X}; \mathbf{A}(\mathbf{c})\theta) \\ &= J_{\mathbf{v}} R(\mathbf{X}; \mathbf{v}) J_{\mathbf{c}} \mathbf{v} \\ &= J_{\mathbf{v}} R(\mathbf{X}; \mathbf{v}) \text{diag}(\theta) \end{aligned} \tag{6}$$

where $\mathbf{v} = \mathbf{A}(\mathbf{c})\theta = \theta \odot \mathbf{c}$. Using (7) one can write $\nabla_{\mathbf{c}} g(\theta, \mathbf{c}) = \text{diag}(\theta) J_{\mathbf{v}}^T R(\mathbf{X}; \mathbf{v})$. Also, by noting the fact that transpose of the Jacobian of a scalar-valued function is the gradient, one can write $\nabla_{\mathbf{c}} g(\theta, \mathbf{c}) = \nabla_{\mathbf{v}} R(\mathbf{X}; \mathbf{v}) \odot \theta = \nabla_{\theta \odot \mathbf{c}} R(\mathbf{X}; \theta \odot \mathbf{c}) \odot \theta$. Remember the goal was to calculate $\nabla_{\mathbf{c}} R(\mathbf{X}; \theta \odot \mathbf{c})|_{\mathbf{c}=\mathbf{1}}$ so one can write the following:

$$\begin{aligned} \nabla_{\mathbf{c}} g(\theta, \mathbf{c})|_{\mathbf{c}=\mathbf{1}} &= \nabla_{\mathbf{c}} R(\mathbf{X}; \theta \odot \mathbf{c})|_{\mathbf{c}=\mathbf{1}} \\ &= \nabla_{\theta \odot \mathbf{c}} R(\mathbf{X}; \theta \odot \mathbf{c})|_{\mathbf{c}=\mathbf{1}} \odot \theta. \end{aligned} \tag{7}$$

Below we show that $\nabla_{\theta \odot \mathbf{c}} R(\mathbf{X}; \theta \odot \mathbf{c})|_{\mathbf{c}=\mathbf{1}} = \nabla_{\theta} R(\mathbf{X}; \theta)$.

³ $\mathbf{1}_A(x) = \{1 \text{ if } x \in A, 0 \text{ if } x \notin A\}$

First note that $\boldsymbol{\theta} \odot \mathbf{c} = [c_1\theta_1, \dots, c_d\theta_d]^\top$. Then, the i -th entry of $\nabla_{\boldsymbol{\theta} \odot \mathbf{c}} R(\mathbf{X}; \boldsymbol{\theta} \odot \mathbf{c})|_{\mathbf{c}=\mathbf{1}}$ can be written as the following:

$$\begin{aligned} \frac{\partial R(\mathbf{X}; \boldsymbol{\theta} \odot \mathbf{c})}{\partial (c_i \theta_i)}|_{\mathbf{c}=\mathbf{1}} &= \lim_{\epsilon \rightarrow 0} \frac{R(\mathbf{X}; \boldsymbol{\theta} \odot \mathbf{c} + \epsilon \mathbf{e}_i) - R(\mathbf{X}; \boldsymbol{\theta} \odot \mathbf{c})}{\epsilon}|_{\mathbf{c}=\mathbf{1}} \\ &= \lim_{\epsilon \rightarrow 0} \frac{R(\mathbf{X}; \boldsymbol{\theta} + \epsilon \mathbf{e}_i) - R(\mathbf{X}; \boldsymbol{\theta})}{\epsilon} \\ &= \frac{\partial R(\mathbf{X}; \boldsymbol{\theta})}{\partial (\theta_i)} \end{aligned} \quad (8)$$

where \mathbf{e}_i is the vector of zeros in \mathbb{R}^d except for the j -th entry which is one. Therefore,

$$\nabla_{\mathbf{c}} g(\boldsymbol{\theta}, \mathbf{c})|_{\mathbf{c}=\mathbf{1}} = \mathbf{s} = \boldsymbol{\theta}^0 \odot \nabla_{\boldsymbol{\theta}} R(\mathbf{X}; \boldsymbol{\theta}^0)$$

Another way of deriving the score in (Lee et al., 2018) would be using the directional derivative. Looking at the problem from this standpoint would be beneficial for deriving the score in (Wang et al., 2020). Recall directional derivative of a scalar-valued function $f(\mathbf{x})$ along vector \mathbf{v} is defined as follows:

$$D_{\mathbf{v}} f(\mathbf{x}) = \lim_{\epsilon \rightarrow 0} \frac{f(\mathbf{x} + \epsilon \mathbf{v}) - f(\mathbf{x})}{\epsilon} = \nabla_{\mathbf{x}}^\top f(\mathbf{x}) \mathbf{v}. \quad (9)$$

As one can observe, Equation (9) is a scalar value and only provides variation of function $f(\mathbf{x})$ along vector \mathbf{v} . This only provides linear change of the function because the perturbation is done only along vector \mathbf{v} and not all directions. Hence, one can write the following for the empirical risk function:

$$D_{\mathbf{v}} R(\mathbf{X}; \boldsymbol{\theta}) = \nabla^\top R(\mathbf{X}; \boldsymbol{\theta}) \mathbf{v} \quad (10)$$

where ∇^\top denotes the transpose of the gradient. At initialization $\boldsymbol{\theta} = \boldsymbol{\theta}^0$ and one may examine variation of the function along each direction of $\boldsymbol{\theta}^0$ separately letting $\mathbf{v} = \theta_i^0 \mathbf{e}_i$ so one has the following:

$$D_{\theta_i^0 \mathbf{e}_i} R(\mathbf{X}; \boldsymbol{\theta}^0) = \left(\nabla^\top R(\mathbf{X}; \boldsymbol{\theta}^0) \right) (\theta_i^0 \mathbf{e}_i) = \left(\nabla^\top R(\mathbf{X}; \boldsymbol{\theta}^0) \right)_i \theta_i^0 \quad (11)$$

where $\left(\nabla^\top R(\mathbf{X}; \boldsymbol{\theta}^0) \right)_i$ is the i -th component of the gradient at $\boldsymbol{\theta}^0$. Each value in Equation (11) for different i is the i -th entry in the score introduced by Lee et al. (2018).

A.1.2 Derivation of GraSP score

In order to have better intuition about GraSP score, one needs to recall that in the course of training, an SGD-style algorithm goes along negative direction of the gradient. Therefore, from Equation (10) one can easily find a change in the function value along that direction by letting $\mathbf{v} = -\nabla R(\mathbf{X}; \boldsymbol{\theta})$ as follows:

$$D_{-\nabla R(\mathbf{X}; \boldsymbol{\theta})} R(\mathbf{X}; \boldsymbol{\theta}) = -\left(\nabla^\top R(\mathbf{X}; \boldsymbol{\theta}) \right) \nabla R(\mathbf{X}; \boldsymbol{\theta}) = -\|\nabla R(\mathbf{X}; \boldsymbol{\theta})\|_2^2 \quad (12)$$

which is a well-known fact stating that change in the function along the opposite direction of the gradient is ℓ_2 norm of the gradient. Now one wants to see the variability of this function along an arbitrary vector $\mathbf{v} = \boldsymbol{\delta}$ so we have:

$$D_{\boldsymbol{\delta}} - \|\nabla R(\mathbf{X}; \boldsymbol{\theta})\|_2^2 = \nabla^\top (-\|\nabla R(\mathbf{X}; \boldsymbol{\theta})\|_2^2) \mathbf{v} = 2 \left(-\mathbf{H} R(\mathbf{X}; \boldsymbol{\theta}) \nabla R(\mathbf{X}; \boldsymbol{\theta})^\top \right) \boldsymbol{\delta} \quad (13)$$

Observe that Equation (13) is a function of two different vectors: $\boldsymbol{\theta}$ and $\boldsymbol{\delta}$. At initialization $\boldsymbol{\theta} = \boldsymbol{\theta}^0$ change in function along each direction of $\boldsymbol{\theta}^0$, i.e., $\boldsymbol{\delta} = \theta_i^0 \mathbf{e}_i$ is the score provided in (Wang et al., 2020).

B Detailed experiments

In this section we provide all the detail results of experiments listed in Table 1. These detail results include test accuracy of four different variants where (D) dense network with $s = 0$, (A) trained with *ASNI* to have sparsity s , (C) sparse network reinitialized by *ASNI* initialization (c_{\pm}), and (S) sparse network reinitialized by the original initialization. Also, for each experiment histogram of network parameters is provided. Furthermore, layer-wise histogram of parameters of a network that is sparsified by *ASNI* is provided. These histograms include centroids and show these centroids are in fact positive and negative means of each layer. Lastly, the layer-wise table showing parameters of each layer, nonzero parameters of each layer and sparsity percentage of each layer is provide for each experiment.

B.1 FC-MNIST

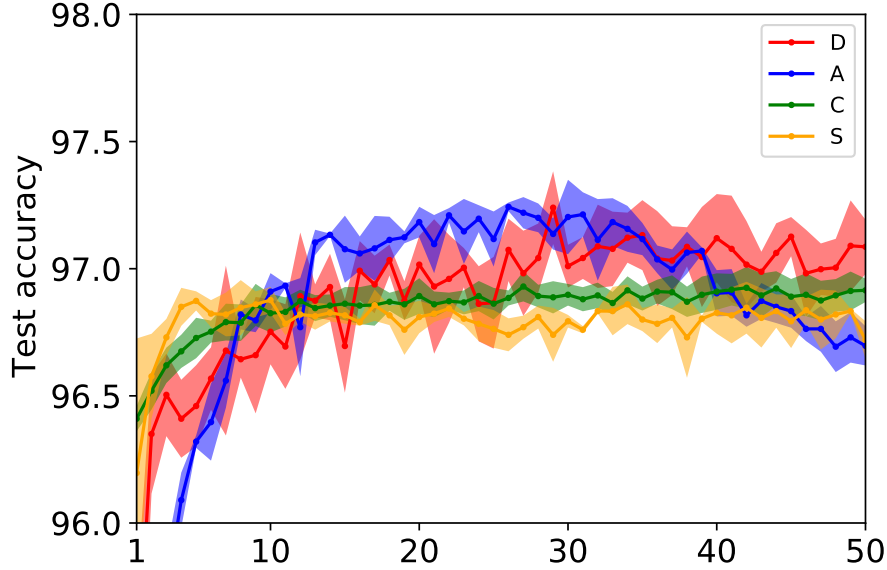


Figure 5: Test accuracy for 4 variants explained in Appendix B.

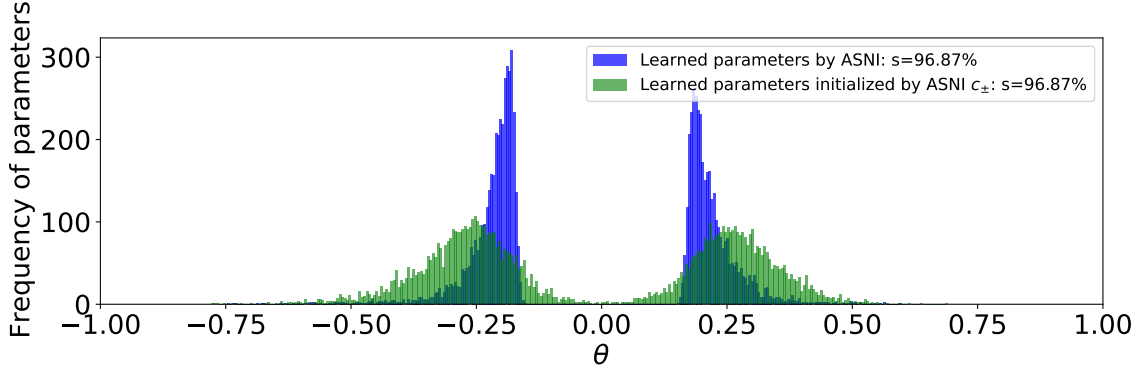


Figure 6: Parameter distribution considering all nonzero parameters of the sparse networks.

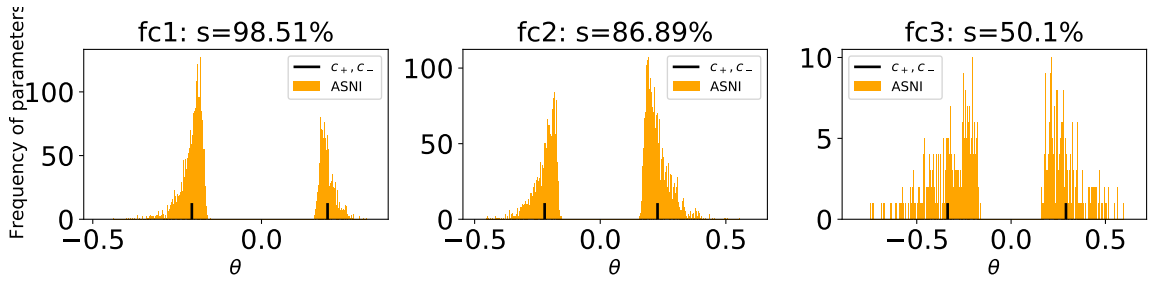


Figure 7: Parameter distribution of each layer.

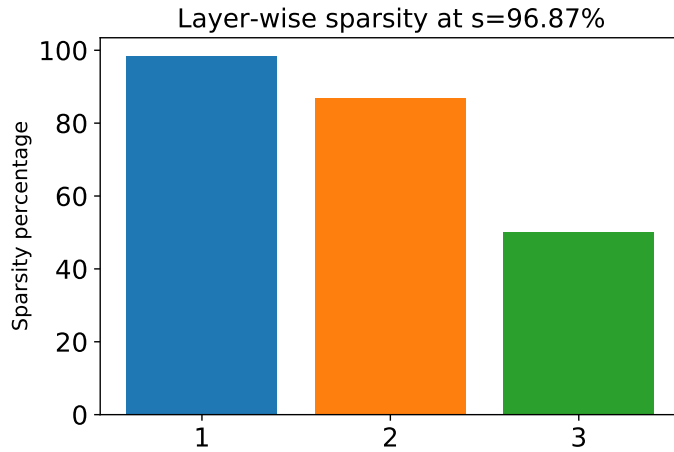


Figure 8: Sparsity distribution across layers.

B.2 Conv2-MNIST

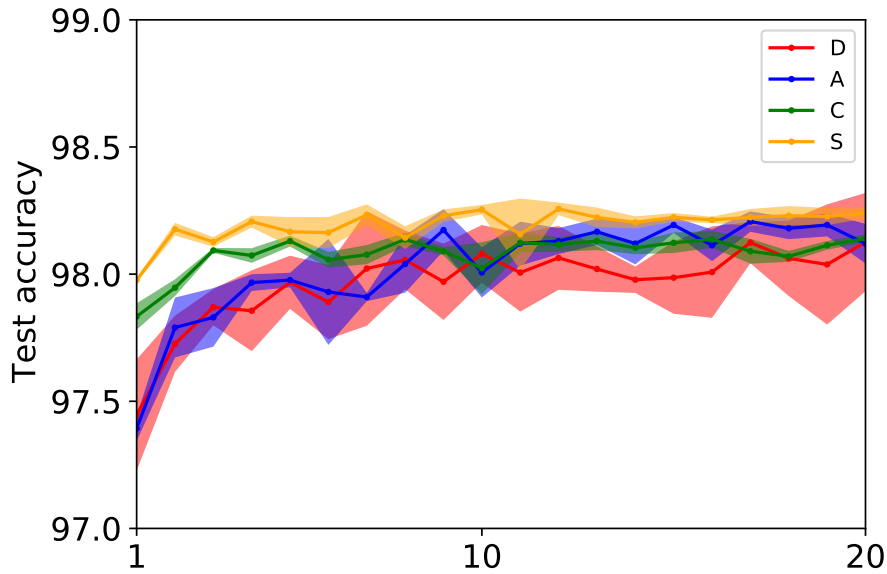


Figure 9: Test accuracy for 4 variants explained in Appendix B.

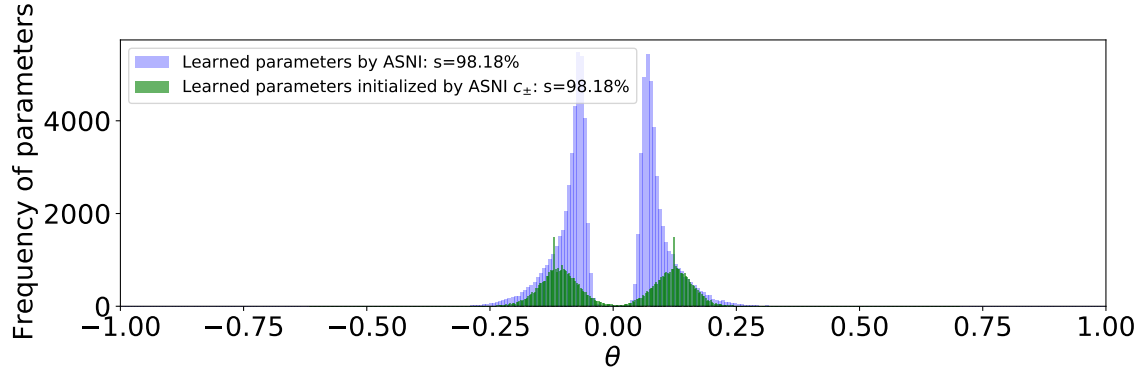


Figure 10: Parameter distribution considering all nonzero parameters of the sparse networks.

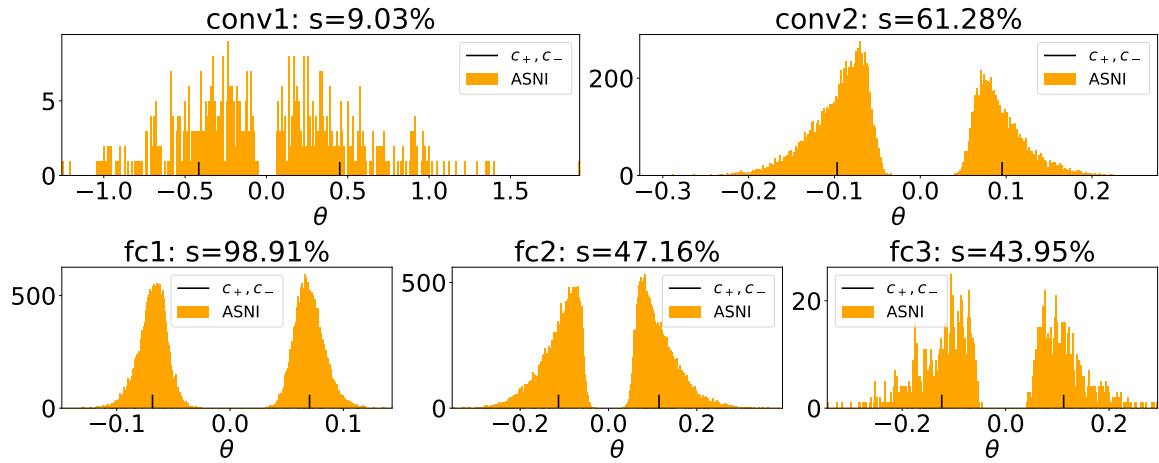


Figure 11: Parameter distribution of each layer.

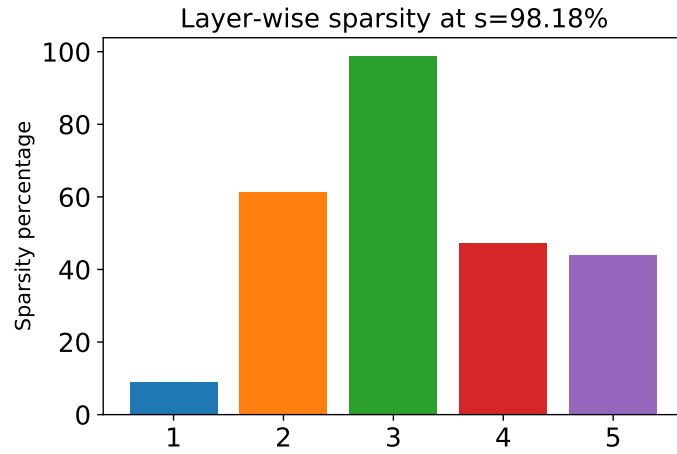


Figure 12: Sparsity distribution across layers.

B.3 Conv4-MNIST

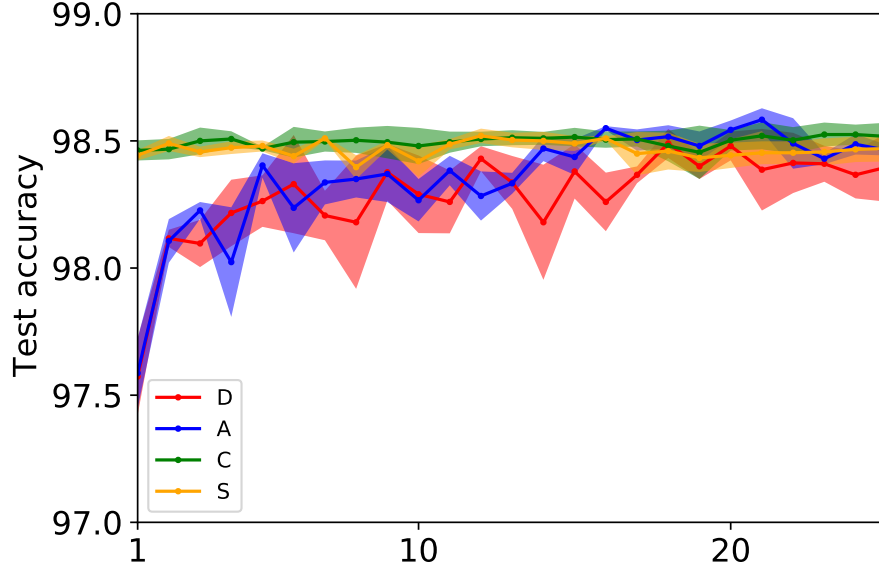


Figure 13: Test accuracy for 4 variants explained in Appendix B.

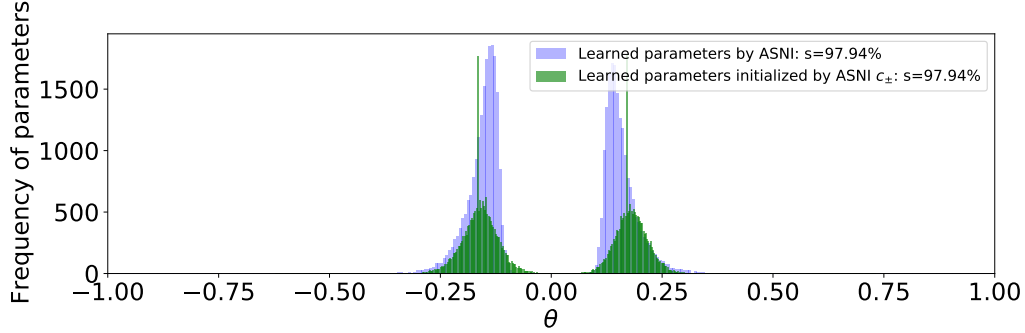


Figure 14: Parameter distribution considering all nonzero parameters of the sparse networks.

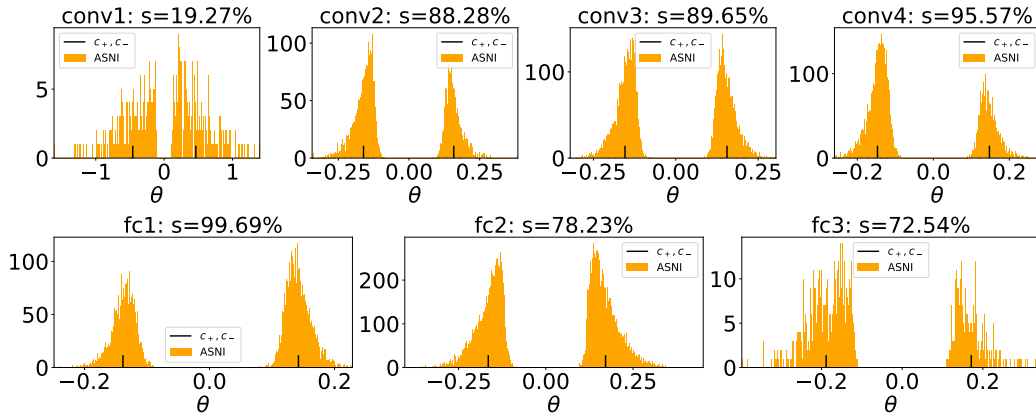


Figure 15: Parameter distribution of each layer.

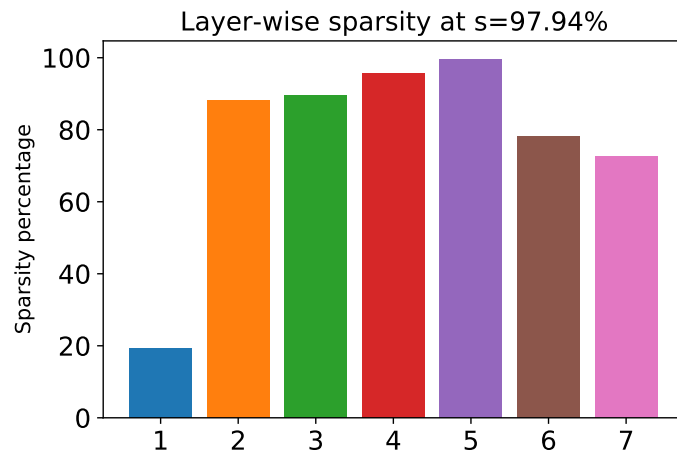


Figure 16: Sparsity distribution across layers.

B.4 Conv6-MNIST

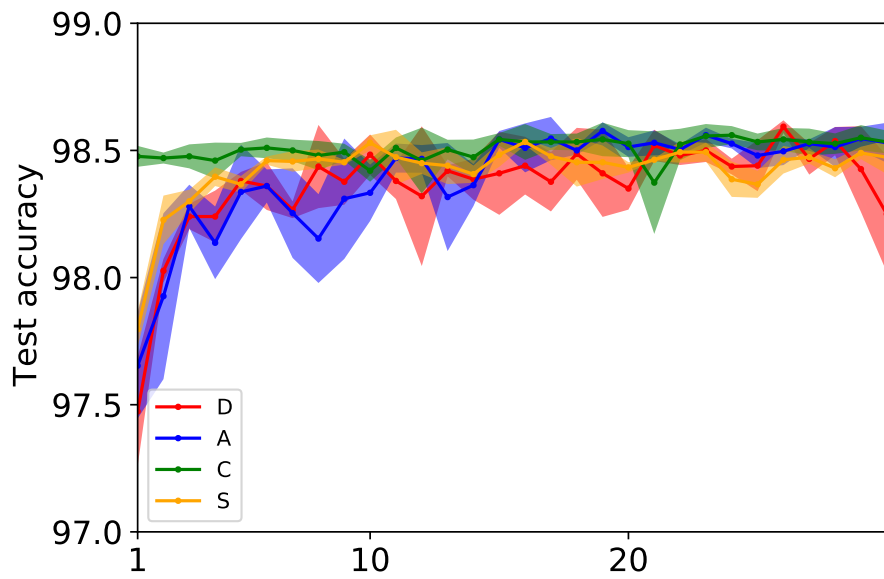


Figure 17: Test accuracy for 4 variants explained in Appendix B.

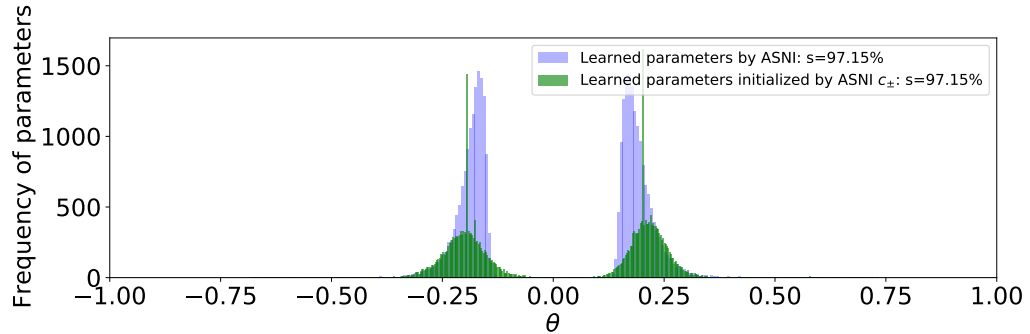


Figure 18: Parameter distribution considering all nonzero parameters of the sparse networks.

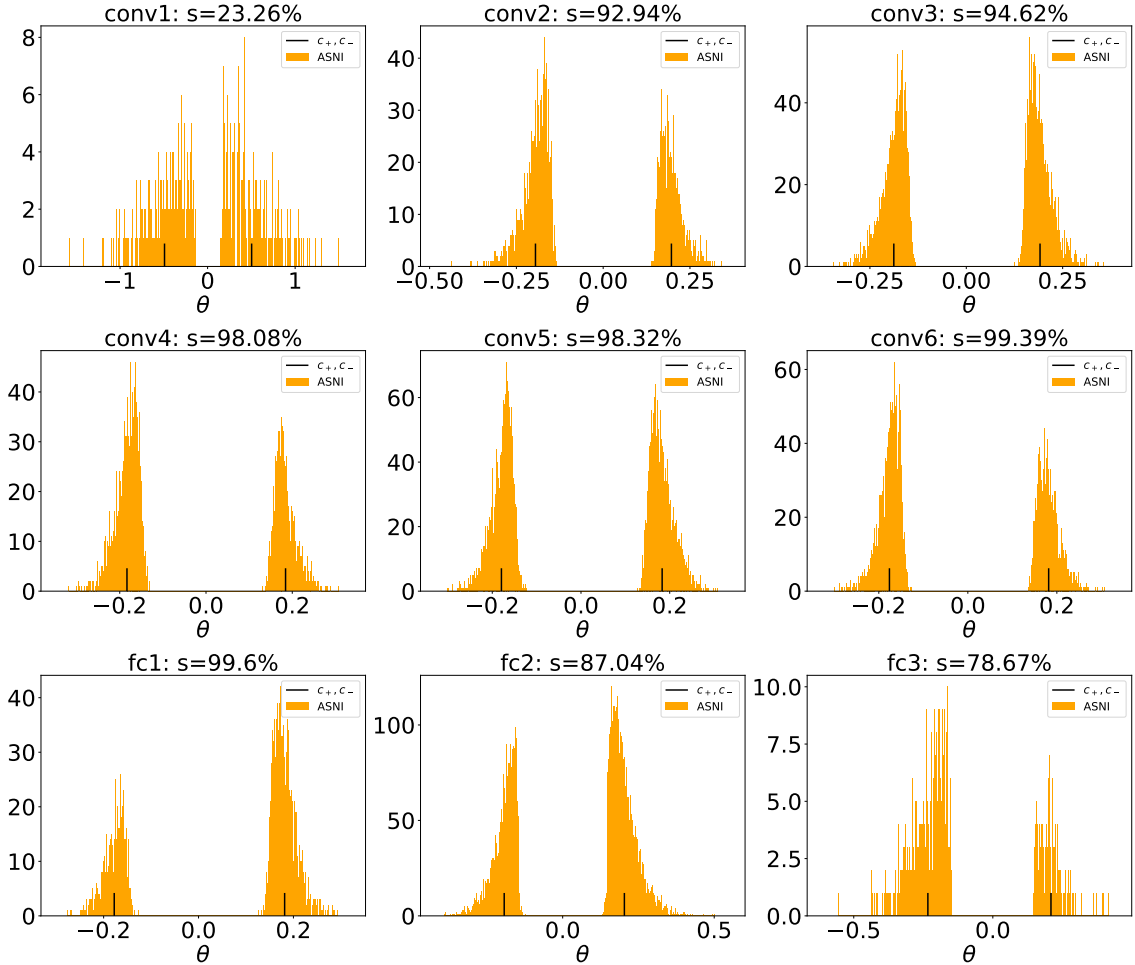


Figure 19: Parameter distribution of each layer.

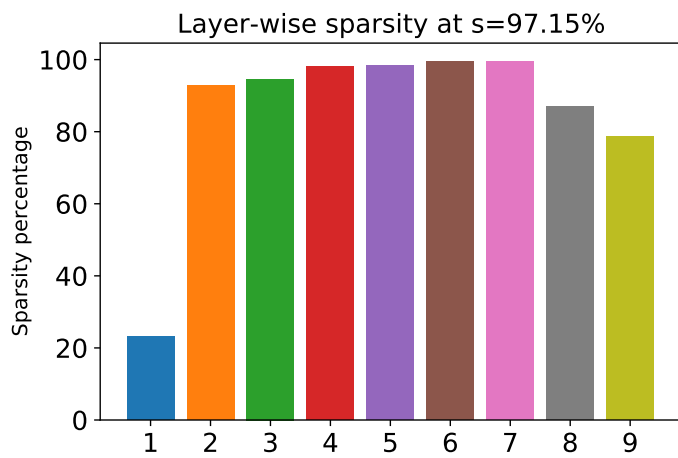


Figure 20: Sparsity distribution across layers.

B.5 Conv2-CIFAR10

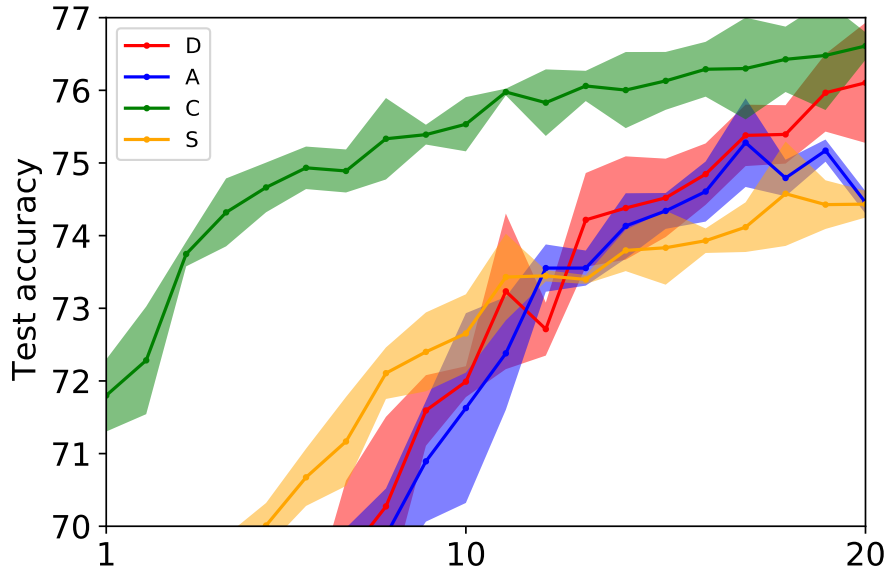


Figure 21: Test accuracy for 4 variants explained in Appendix B.

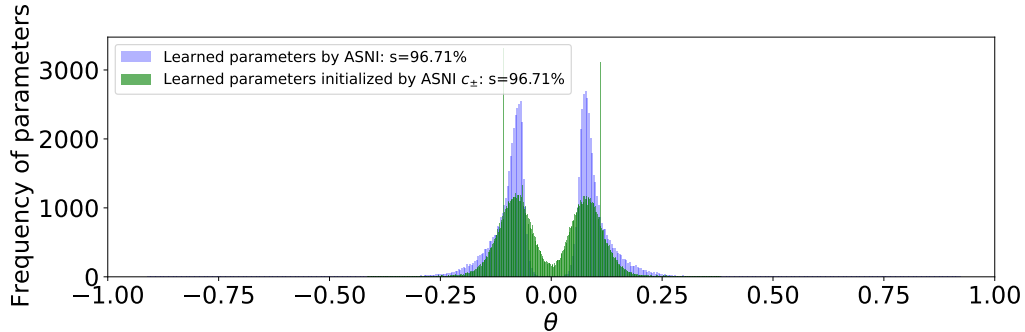


Figure 22: Parameter distribution considering all nonzero parameters of the sparse networks.

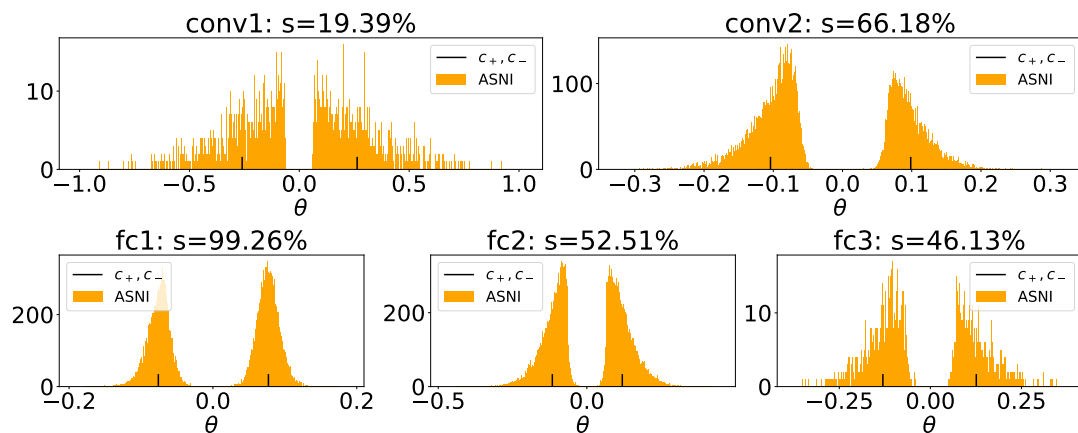


Figure 23: Parameter distribution of each layer.

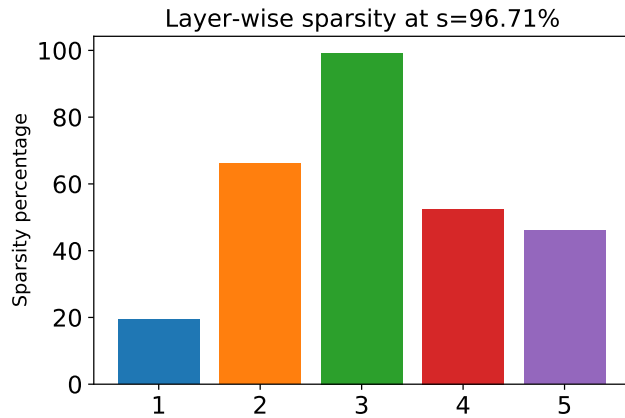


Figure 24: Sparsity distribution across layers.

B.6 Conv4-CIFAR10

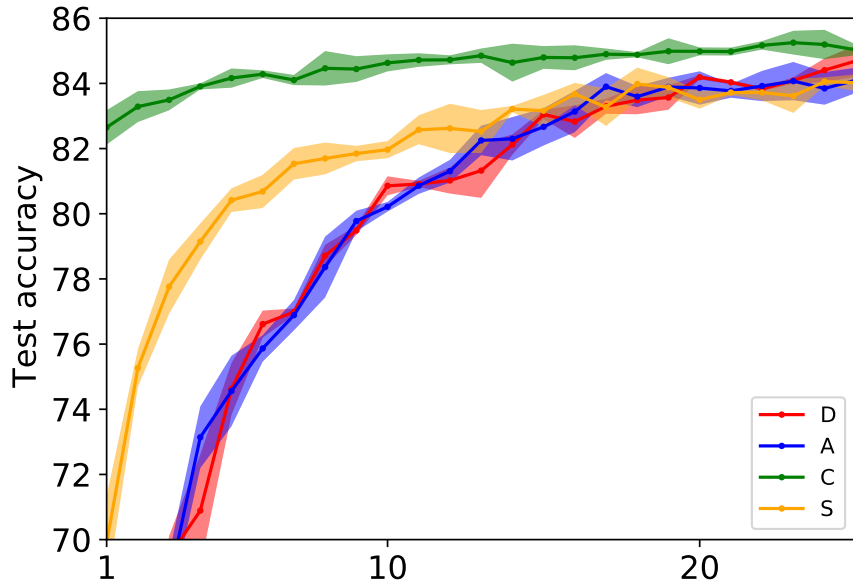


Figure 25: Test accuracy for 4 variants explained in Appendix B.

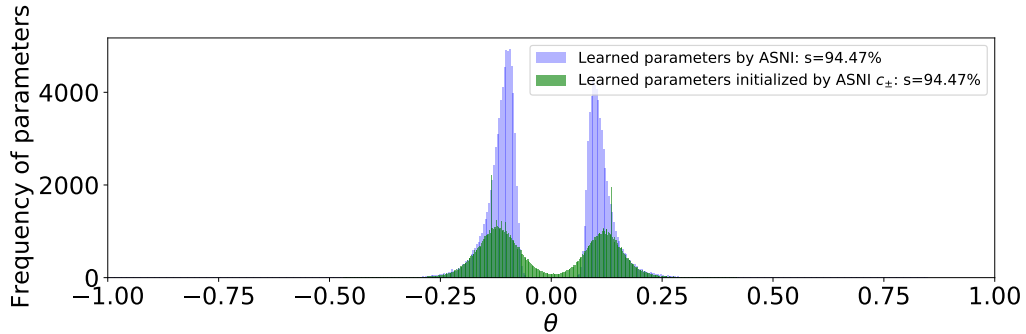


Figure 26: Parameter distribution considering all nonzero parameters of the sparse networks.

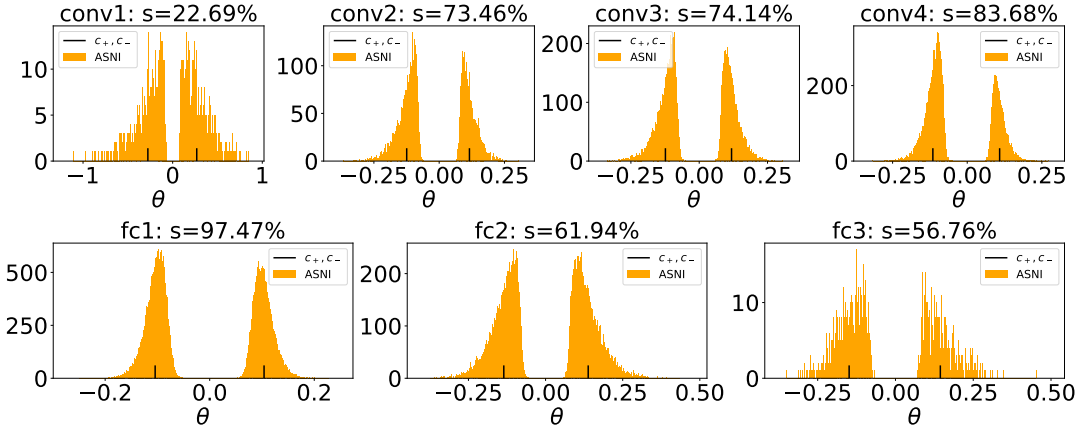


Figure 27: Parameter distribution of each layer.

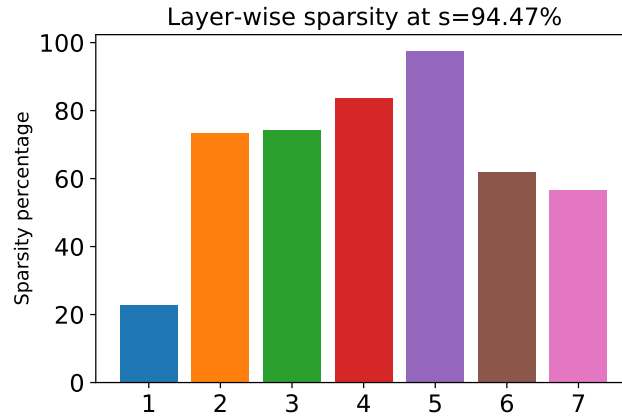


Figure 28: Sparsity distribution across layers.

B.7 Conv6-CIFAR10

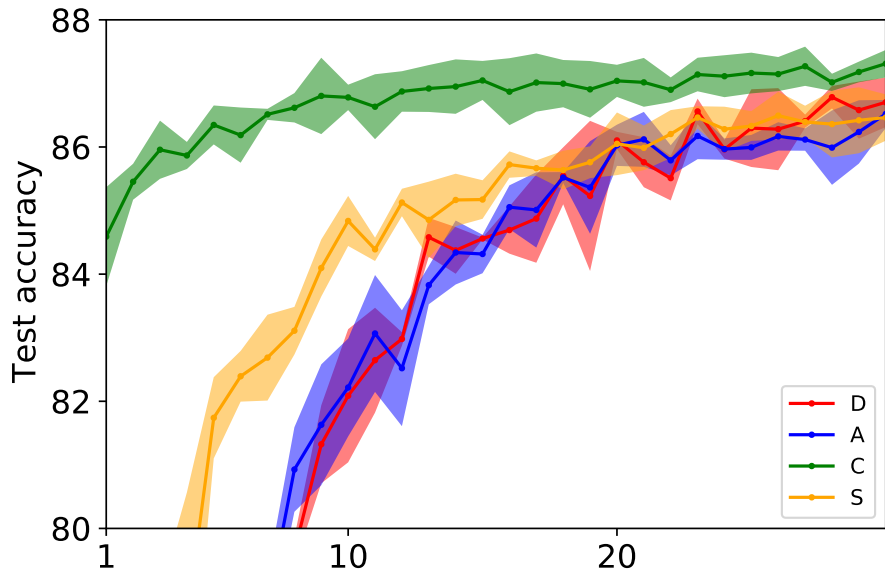


Figure 29: Test accuracy for 4 variants explained in Appendix B.

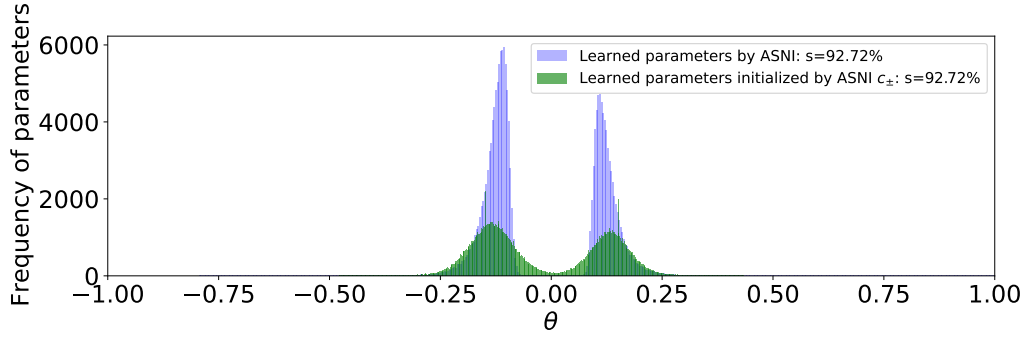


Figure 30: Parameter distribution considering all nonzero parameters of the sparse networks.

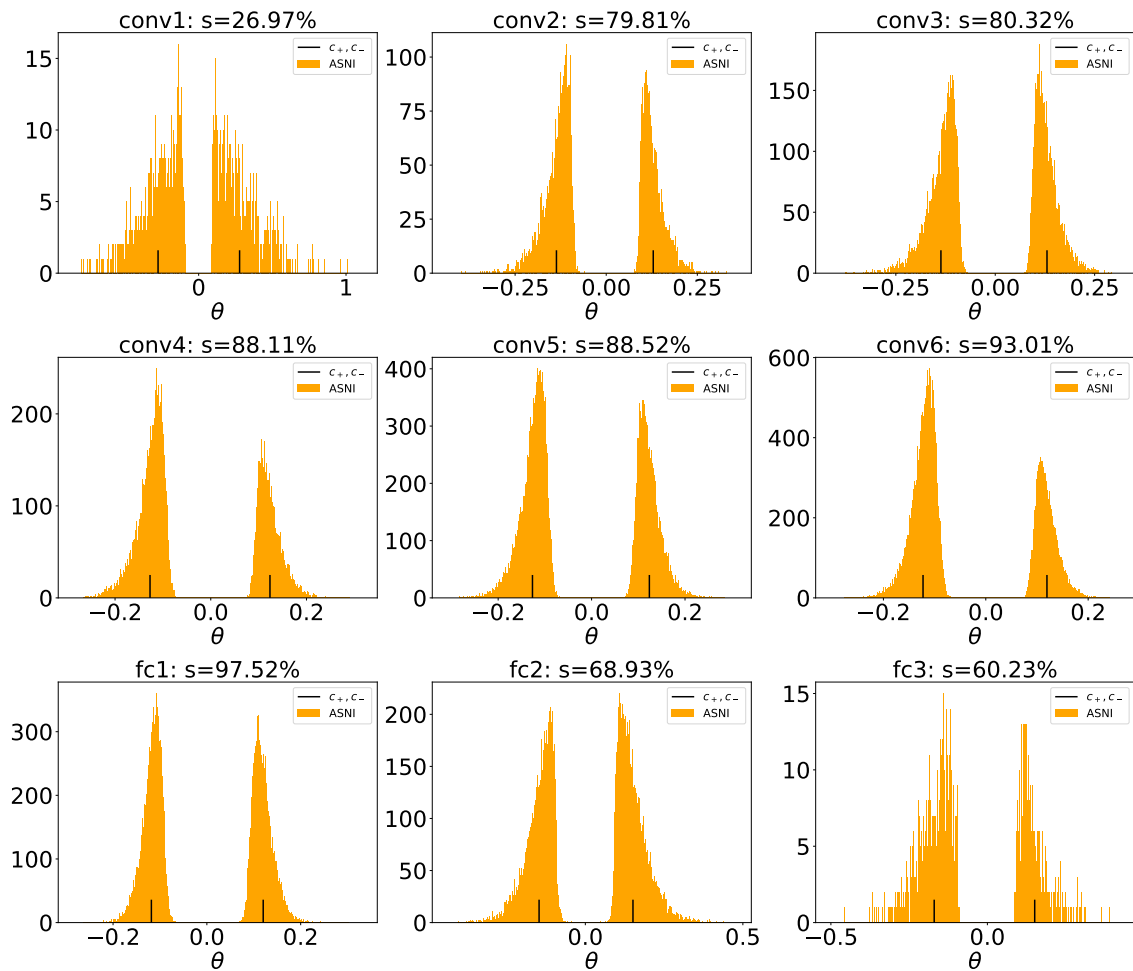


Figure 31: Parameter distribution of each layer.

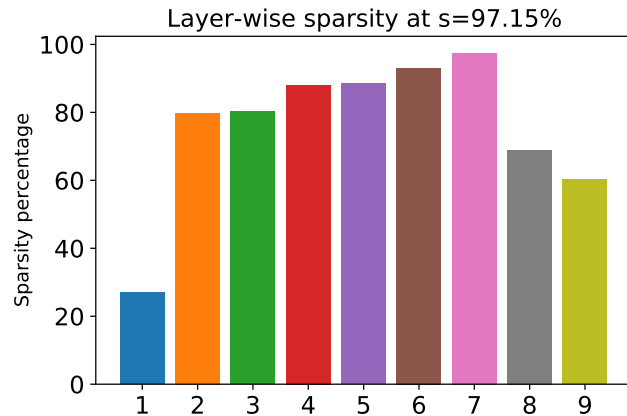


Figure 32: Sparsity distribution across layers.

B.8 VGG11-CIFAR10

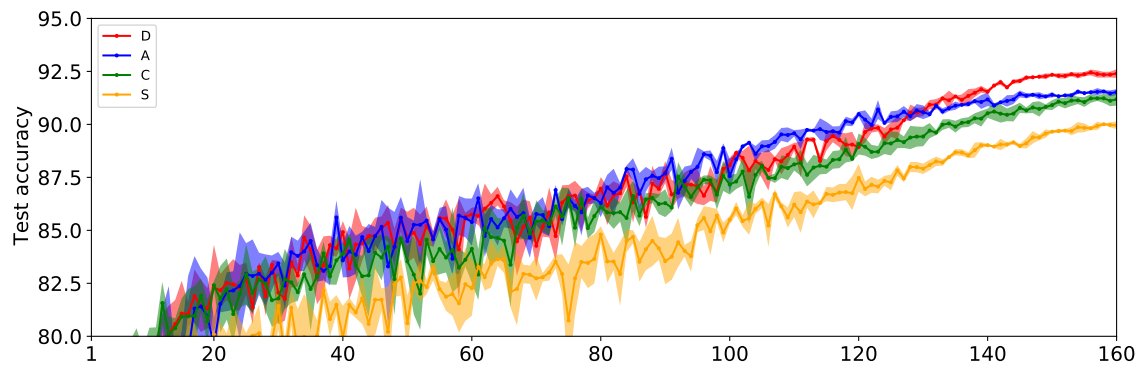


Figure 33: Test accuracy for 4 variants explained in Appendix B.

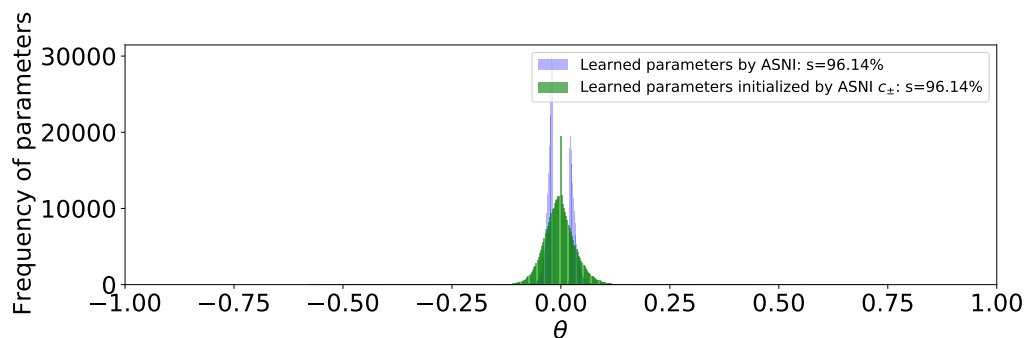


Figure 34: Parameter distribution considering all nonzero parameters of the sparse networks.

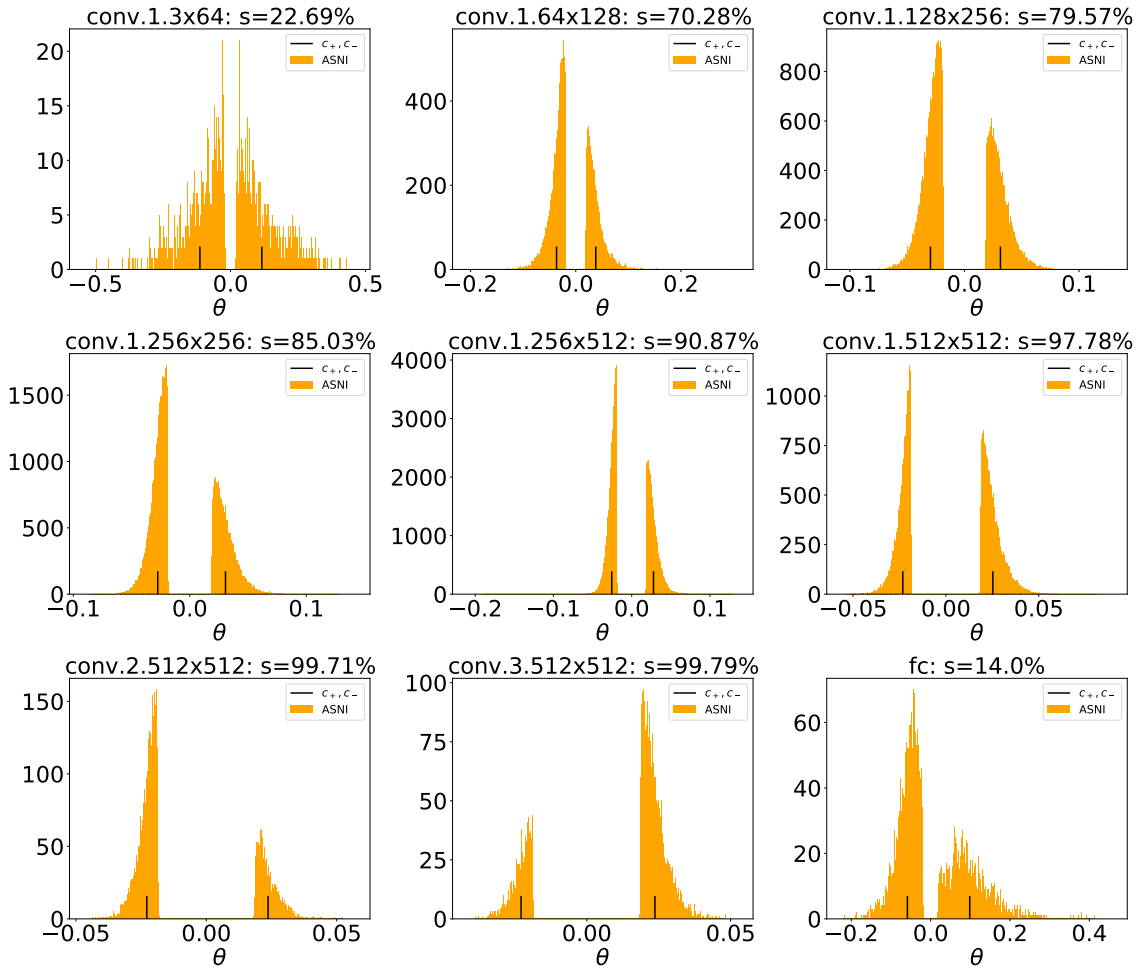


Figure 35: Parameter distribution of each layer.

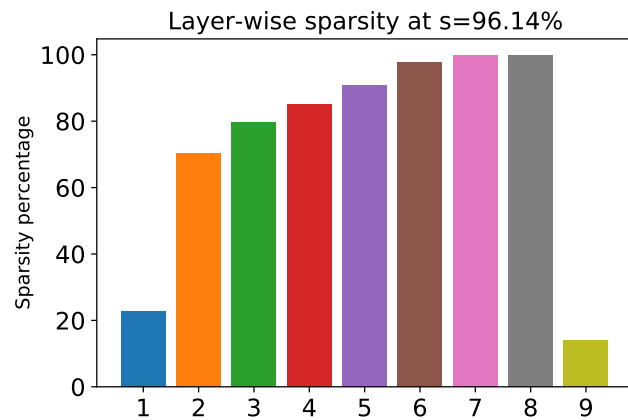


Figure 36: Sparsity distribution across layers.

B.9 VGG13-CIFAR10

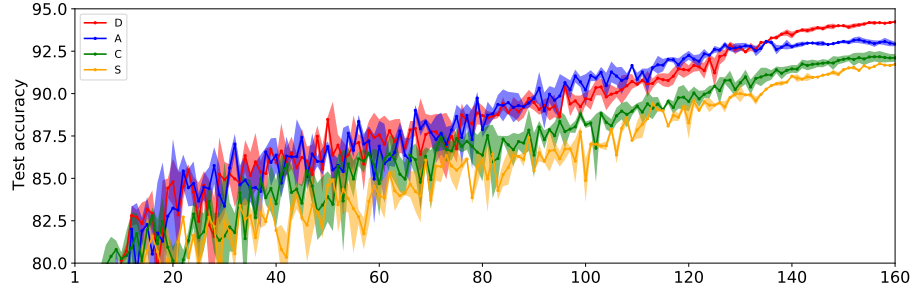


Figure 37: Test accuracy for 4 variants explained in Appendix B.

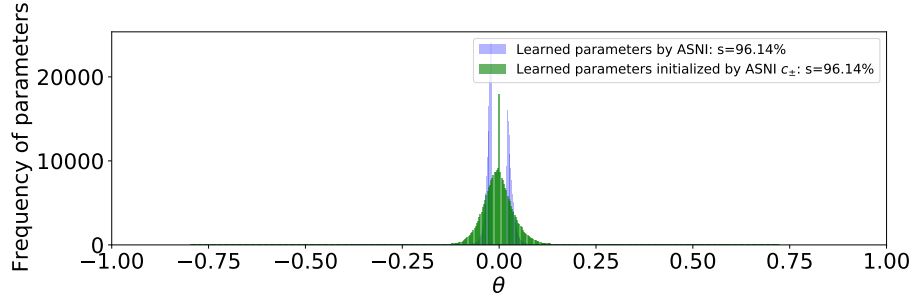


Figure 38: Parameter distribution considering all nonzero parameters of the sparse networks.

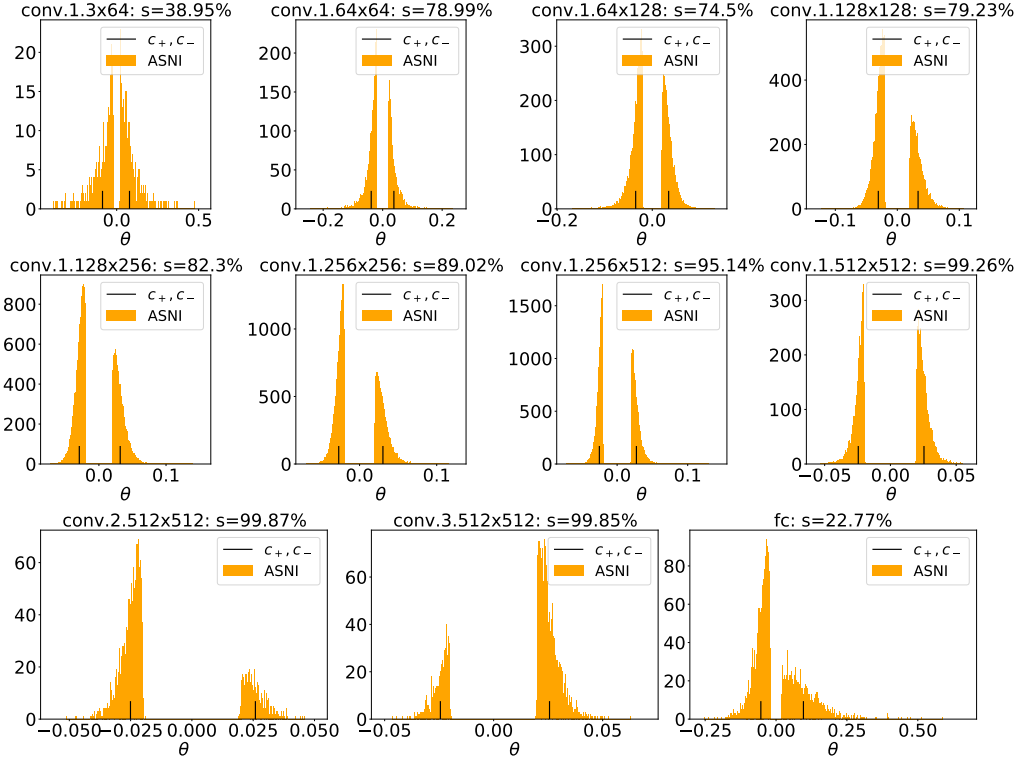


Figure 39: Parameter distribution of each layer.

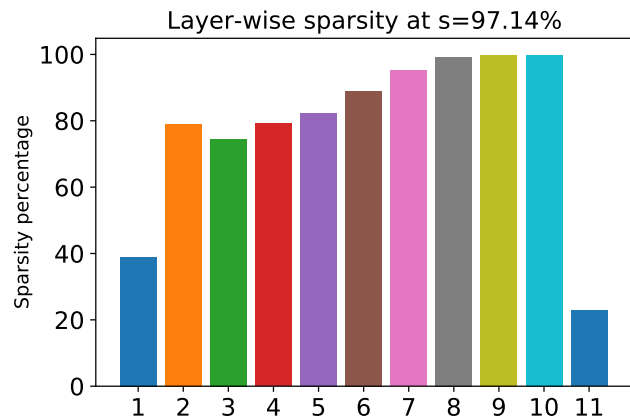


Figure 40: Sparsity distribution across layers.

B.10 VGG16-CIFAR10

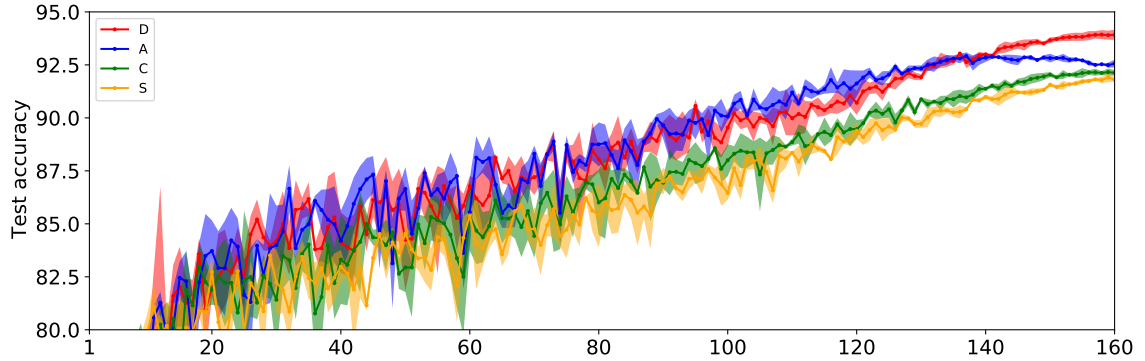


Figure 41: Test accuracy for 4 variants explained in Appendix B.

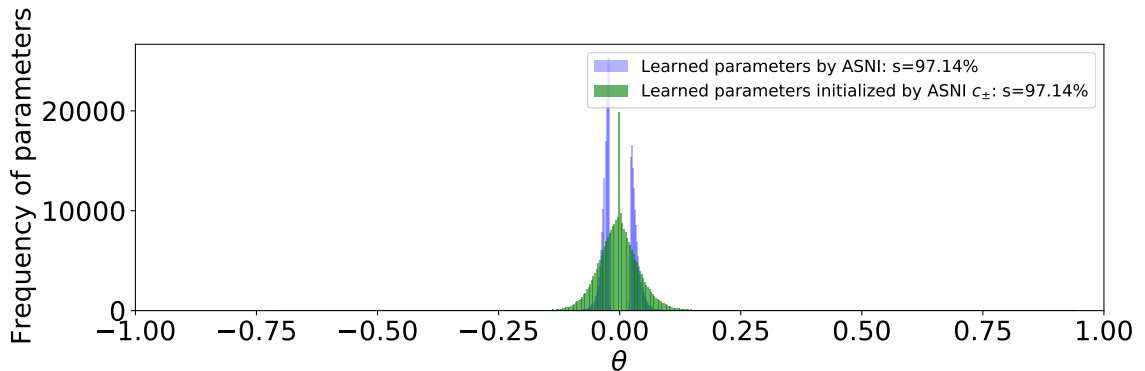


Figure 42: Parameter distribution considering all nonzero parameters of the sparse networks.

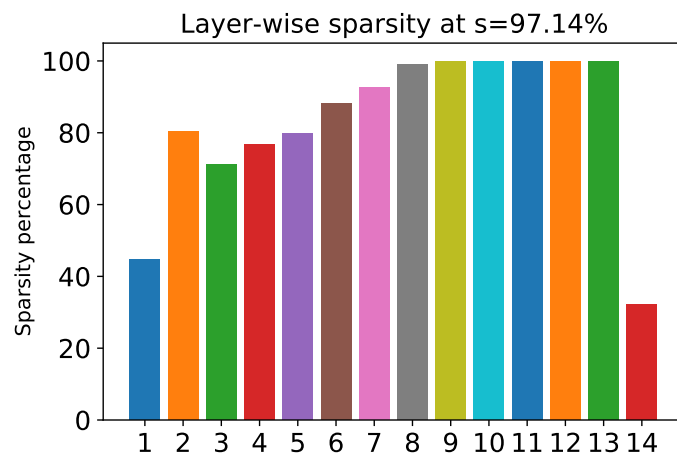


Figure 43: Sparsity distribution across layers.

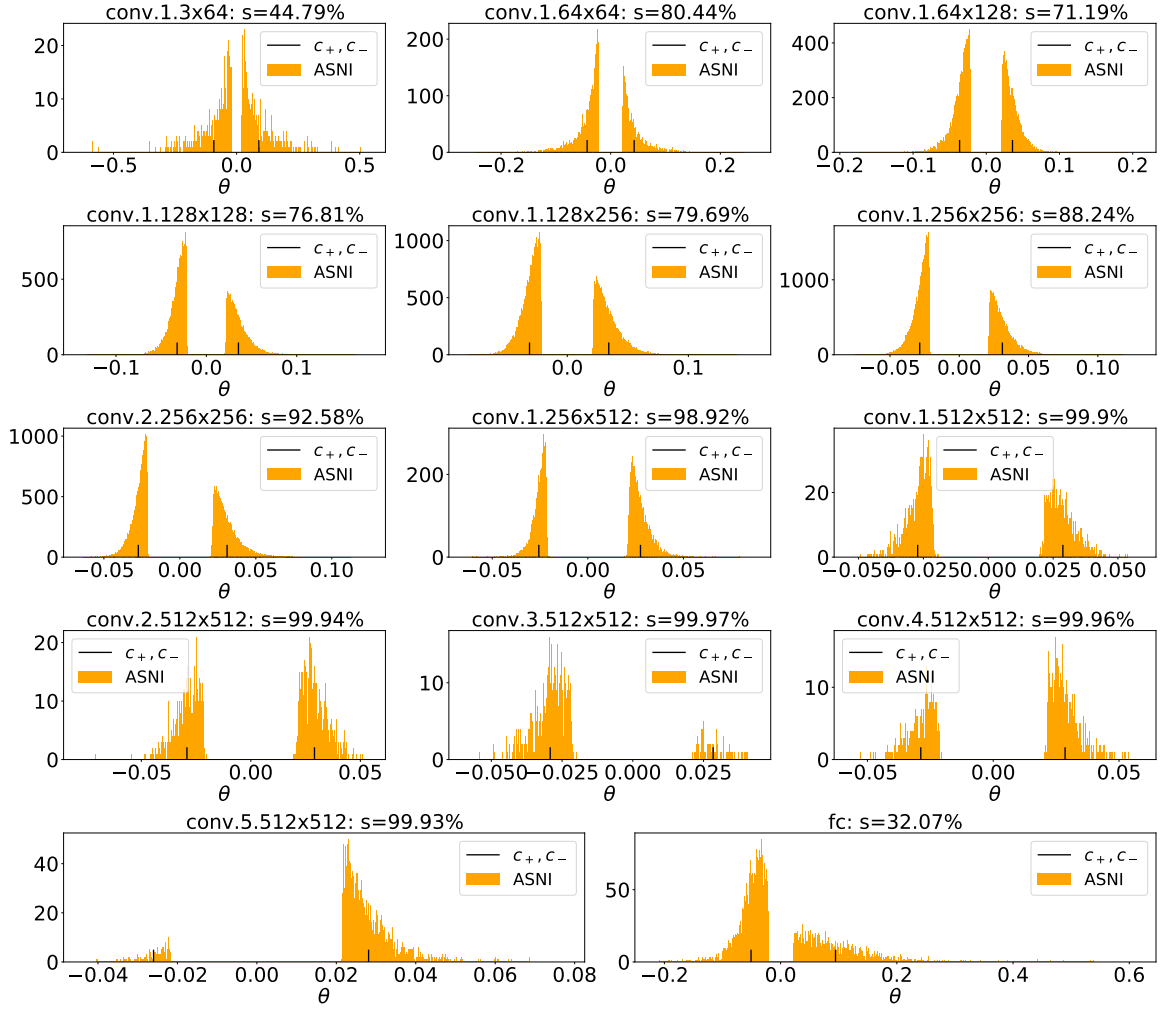


Figure 44: Parameter distribution of each layer.

B.11 ResNet18-CIFAR10

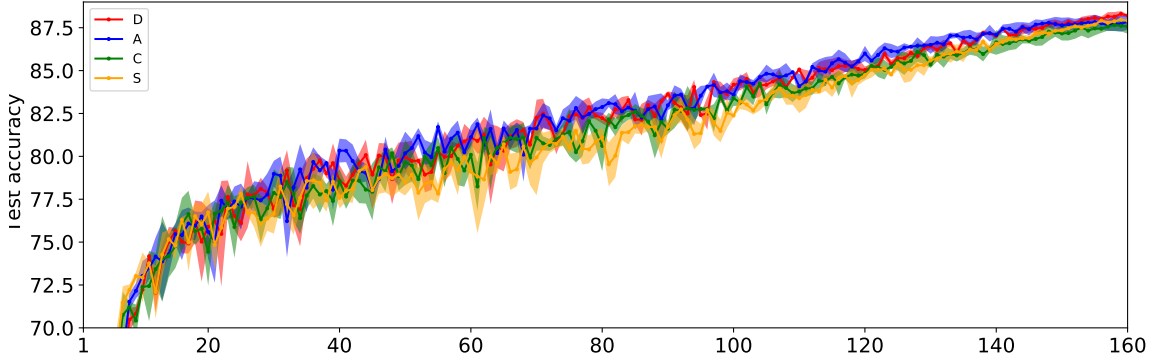


Figure 45: Test accuracy for 4 variants explained in Appendix B.

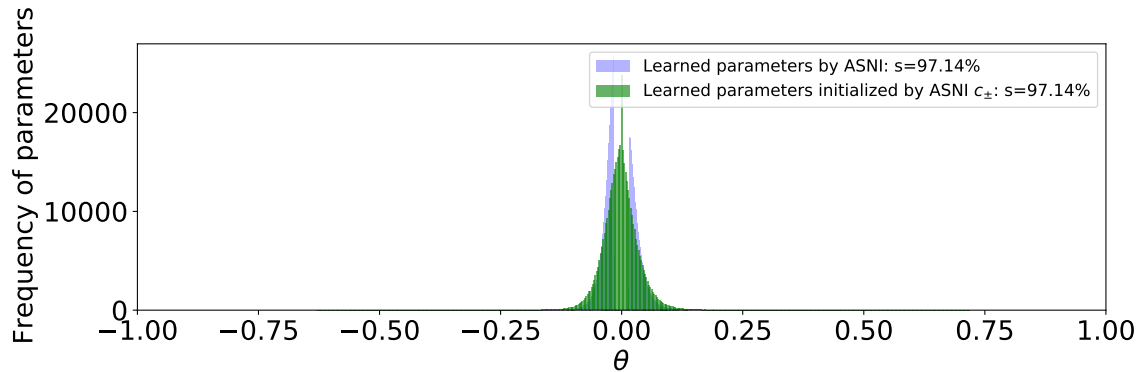


Figure 46: Parameter distribution considering all nonzero parameters of the sparse networks.

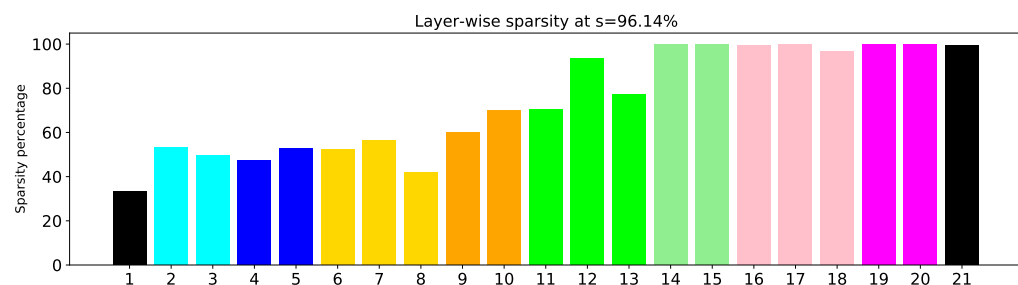


Figure 47: Sparsity distribution across layers.

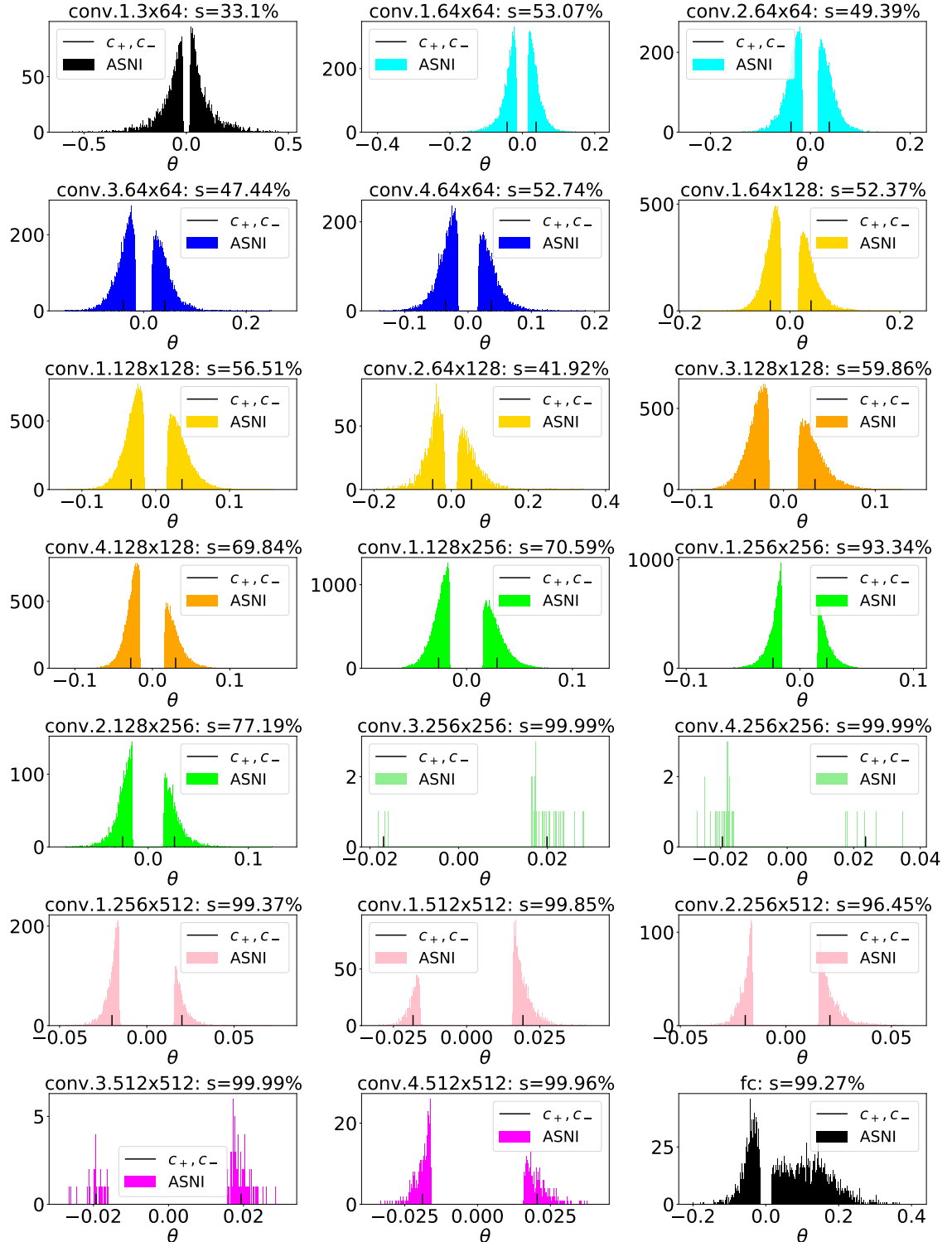


Figure 48: Parameter distribution of each layer.

B.12 ResNet50-ImageNet-1K

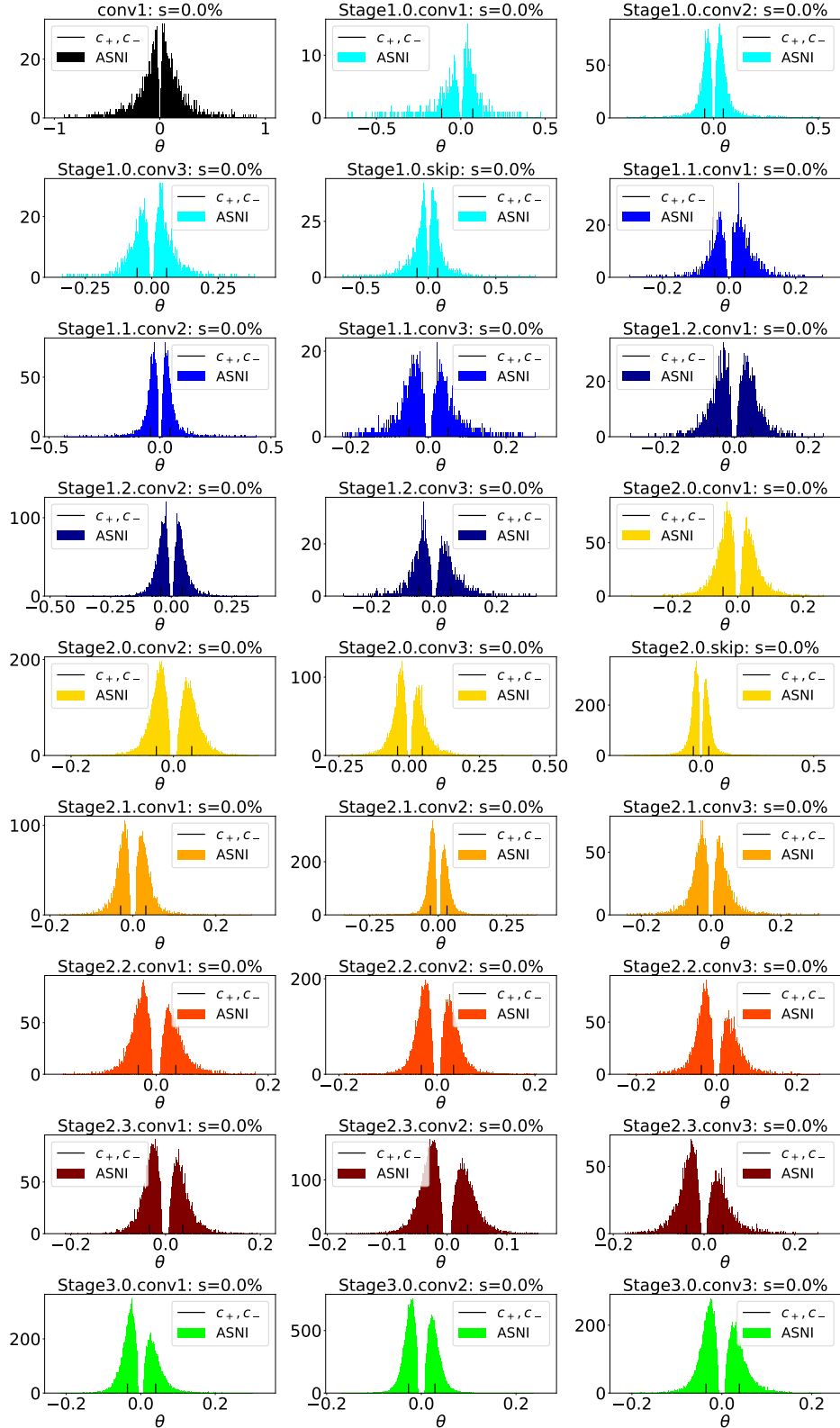


Figure 49: Parameter distribution of each layer.

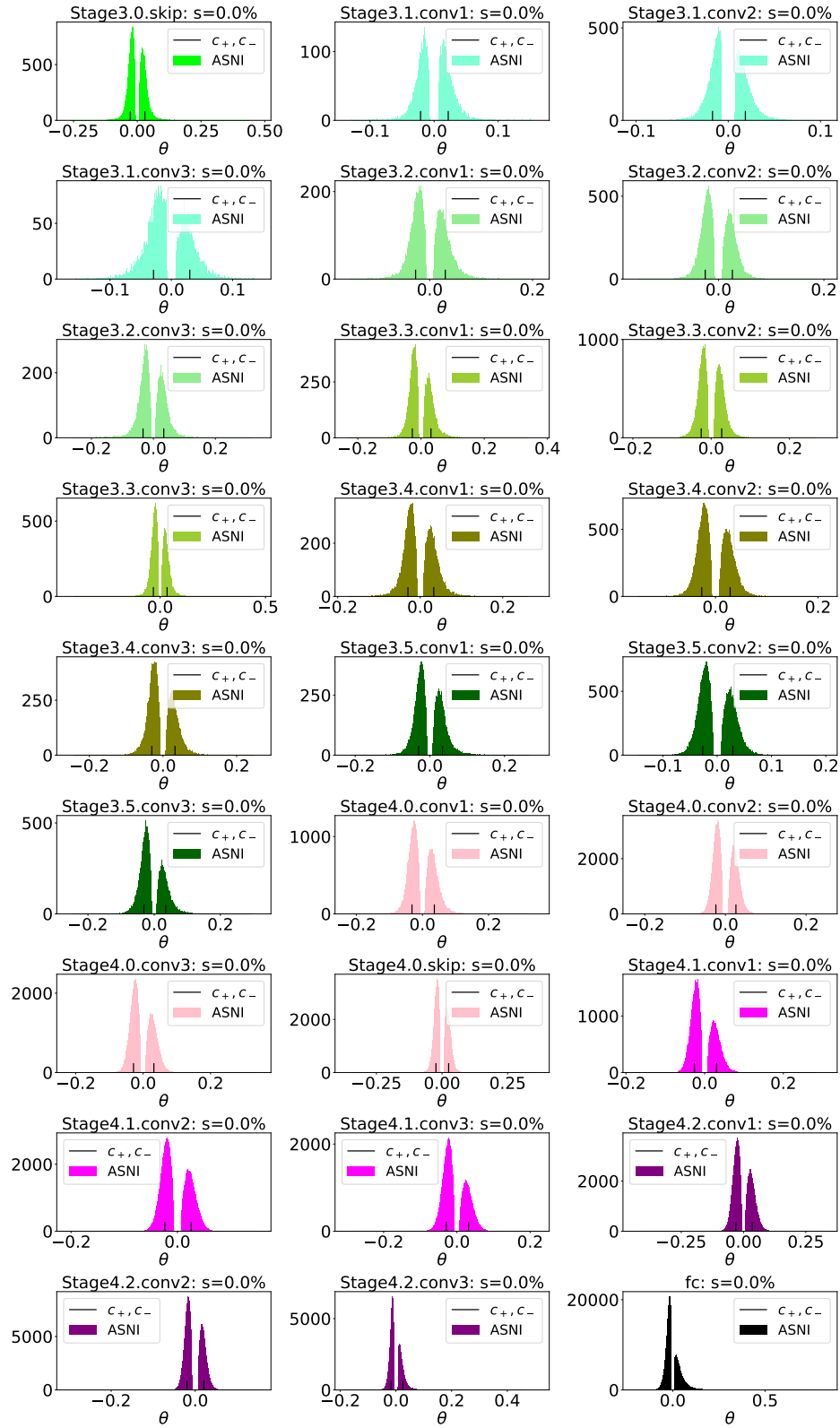


Figure 50: Parameter distribution of each layer.